12-2005

Topology Optimization of Carbon Nanotube Reinforced Polymer Damping Structures

Seshadri Mohan Varma Damu
University of Tennessee - Knoxville

To the Graduate Council:

I am submitting herewith a thesis written by Seshadri Mohan Varma Damu entitled "Topology Optimization of Carbon Nanotube Reinforced Polymer Damping Structures." I have examined the final electronic copy of this thesis for form and content and recommend that it be accepted in partial fulfillment of the requirements for the degree of Master of Science, with a major in Mechanical Engineering.

Arnold Lumsdaine, Major Professor

We have read this thesis and recommend its acceptance:

J.A.M.Boulet, William.R.Hamel

Accepted for the Council:
Carolyn R. Hodges

Vice Provost and Dean of the Graduate School

(Original signatures are on file with official student records.)

To the Graduate Council:

I am submitting herewith a thesis written by Seshadri Mohan Varma Damu entitled "Topology Optimization of Carbon Nanotube Reinforced Polymer Damping Structures" I have examined the final electronic copy of this thesis for form and content and recommend that it be accepted in partial fulfillment of the requirements for the degree of Master of Science, with a major in Mechanical Engineering.

Arnold Lumsdaine
Major Professor

We have read this thesis
and recommend its acceptance:

J.A.M.Boulet.

William.R.Hamel.

Accepted for the Council:

Anne Mayhew
Vice Chancellor and
Dean of Graduate Studies

(Original signatures are on file with official student records)

Topology Optimization of Carbon Nanotube Reinforced Polymer Damping Structures

A Thesis
Presented for the
Master of Science
Degree
The University of Tennessee,
Knoxville

Seshadri Mohan Varma Damu

December 2005

Acknowledgments

I wish to thank all those who helped me in completing my Master of Science in Mechanical Engineering. Special thanks go to Dr. Arnold Lumsdaine. Without his input, motivation and knowledge this work would not have been possible. He has been a great professor, mentor and advisor. I thank Dr. J.A.M.Boulet and Dr. William.R.Hamel for being in my thesis committee and providing me with their valuable suggestions. I would also like to thank my family and friends for supporting me throughout this past two years.

Abstract

Topology optimization has been successfully used for improving vibration damping in constrained layer damping structures. Reinforcing carbon nanotubes in a polymer matrix greatly influence the mechanical properties of the polymer. Such nanotube-reinforced polymers (NRP) can be used to further enhance the damping properties of the constrained layer structures. In this work, topology optimization is performed on constrained damping layer structures using NRP in order to maximize the loss factor for the first resonance frequency of the base beam. In addition to the material fractions of the NRP and elastic material, the volume fraction of the nanotubes in the polymer is also a design variable in the optimization process. The modal strain energy method is used for the loss factor calculation. A commercially available finite element code ABAQUS is used for the finite element analysis. The structure is discretized using 2-dimensional 8-noded quadratic elements. Optimization is performed with a gradient based optimization code which uses a sequential quadratic programming algorithm. To make the optimization process more efficient, an analytical method to calculate the gradients is derived to replace the previously used finite difference method. The resulting structures show a remarkable increase in damping performance. To show the robustness of the optimization process, material fraction and base beam thickness parameter studies are also performed.

Table of Contents

List of Tables

List of Figures

Nomenclature

NRP	Nanotube reinforced polymer
CNT	Carbon nanotube
ρ_{NT}	Density of carbon nanotube
ρ_v	Density of viscoelastic material
v_f	Volume fraction of nanotubes
E_{NT}	Stiffness modulus of carbon nanotube
E_v	Stiffness modulus of viscoelastic material
σ	Stress
ε	Strain
E^*	Complex modulus
E'	Elastic or storage modulus
E''	Loss modulus
η_c	Core or material loss factor
G^*	Complex shear modulus

K^*	Complex Bulk modulus
v^*	Complex Poisson's ratio
η	System loss factor
D	Energy dissipated per cycle
W	Total energy per cycle
U_u	Portion of strain energy attributable to the viscoelastic core (complex quantity)
U	Strain energy of the system
$[\mathbf{M}]$	Mass matrix of the system
$[\mathbf{C}]$	Damping matrix
$[\mathbf{K}]$	Stiffness matrix
U_V	Strain energy of viscoelastic elements calculated from purely elastic analysis
U_E	Strain energy of elastic elements
$\mathbf{\Phi}$	Eigen vector or mode shape

$[\mathbf{K}^V]$	Stiffness matrix of viscoelastic elements obtained from purely elastic analysis
$[\mathbf{K}^E]$	Stiffness matrix of elastic elements
ω_d	Damped natural frequency
ω_1 and ω_2	Frequencies at half power points
x_i^v	Fraction of NRP material of the element *"i"*
x_i^e	Fraction of elastic material of the element *"i"*
f_v	Total fraction of NRP material
f_e	Total fraction of elastic material
n	The number of NRP elements (which is equal to the number of elastic elements).
v_f	Volume fraction of carbon nanotubes in the polymer material
Δx_i	Step size
$\frac{\partial f(x)}{\partial x_i}$	Gradient of the objective function with respect to the i^{th} design variable

$f(x + \Delta x)$ Change in the objective function due to a small change in the *i*th variable.

X $[\, x_1 \quad x_2 \quad x_3 \quad \ldots x_n \,]^T$ where, x_i is the i^{th} design variable.

$\mathbf{K}_i^V, \mathbf{K}_i^B \quad \mathbf{K}_i^E$ Elemental stiffness matrices of the *i*th viscoelastic element, *i*th elastic element in the base beam and *i*th elastic element in the design space respectively.

$\mathbf{\Phi}_{iV}$ Part of the eigenvector for *i*th viscoelastic element

$\mathbf{\Phi}_{iB}$ Part of the eigenvector for ith elastic element in the base beam element

$\mathbf{\Phi}_{iE}$ Part of the eigenvector for *i*th elastic element in the design space

p Number of viscoelastic elements = number of elastic elements in the design space.

b Number of elastic elements in the base beam.

CHAPTER 1: INTRODUCTION

Unwanted vibrations in engineering applications can have adverse affects ranging from being mildly annoying to being extremely dangerous. These are a hindrance to performance of machinery and cause human discomfort. Excessive vibrations also cause noise and material fatigue. Vibrations in structures with insufficient damping can result in loss of life and property.

Vibrations in dynamic systems can be reduced by a number of means. Damping by absorption, isolation, air damping, magnetic hysteresis, particle damping, fluid viscosity and piezoelectric damping are a few such methods. In structural applications, one common form of damping employed to reduce noise and vibration is using viscoelastic laminates, usually in the form of an add-on treatments applied to a structure.

Damping refers to the extraction of mechanical energy from a vibrating system usually by conversion into heat. Internal damping and structural damping are two general forms of damping in structures. Internal damping or material damping refers to the mechanical energy dissipation within the material and structural damping refers to damping at supports, joints, interfaces etc. Most engineering structural applications have very little internal damping. In such cases, applying a viscoelastic layer on the structure is one of the easiest and most cost effective methods of vibration damping. Vibration damping using viscoelastic materials can be classified as either free or constrained layer damping treatment.

Free layer damping involves bonding the damping material to the structure, usually using a pressure sensitive adhesive. When the base structure deforms in bending,

the viscoelastic material deforms primarily in extension as shown in figure 1.1. The degree of damping is limited by the thickness and weight restrictions. In the vibration analysis of a beam with a viscoelastic layer conducted by Kerwin (1959), it was seen that the system loss factor of a free layer system increases with the thickness and loss factor of the viscoelastic layer.

In constrained layer damping treatment, there is an additional constraining layer on top of the viscoelastic layer as shown in figure 1.2. In this case, the energy dissipation occurs primarily by shear. Ross et al. (1959) performed analytical and experimental studies of constrained layer damping structures using viscoelastic materials. They showed that shear damping (constrained layer damping) is a more effective method than free layer damping.

1.1 Literature Survey

One of the first analytical studies of unconstrained layer beams was conducted by Oberst and Frankenfeld (1952). Commonly used methods for analysis of free layer and

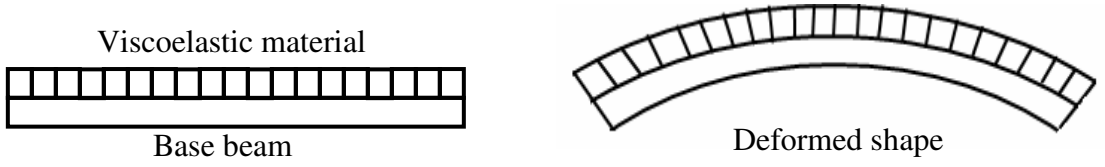

Figure 1.1 Free layer damping

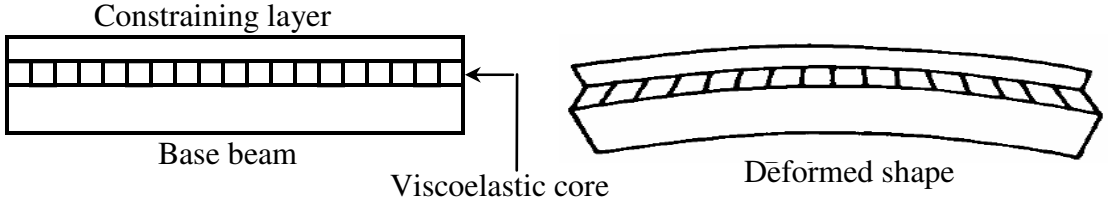

Figure 1.2 Constrained layer damping

constrained layer treatments were developed by Kerwin (1959) and Ross et al. (1959), respectively. These were fourth-order bending equations developed assuming sinusoidal expansions for the modes of vibration applicable to simply supported beams. A more general sixth-order equation of motion for arbitrary boundary conditions was derived by DiTaranto (1965) and Mead and Markus (1969). Rao (1978) developed a set of equationsof motion and boundary conditions for the vibration of sandwich beams using an energy approach. Numerous other studies were reviewed by Nakra (1976, 1981 and 1984).

Finite elements have commonly been employed to characterize laminated structures (for example, see Hwang et al. 1992). Ungar and Kerwin (1962) introduced the concept of damping in terms of strain energy quantities. The implementation of the strain energy method in finite element form to predict the loss factor of composite structures was first demonstrated by Johnson and Kienholz (1981). They introduced the modal strain energy method which is now widely used. Soni and Bogner(1982) used a finite element computer program, MAGNA-D to predict the response of damped structures to steady state inputs.

Methods to predict the damping in fiber-reinforced polymer composites have also been investigated. Schultz and Tsai (1968) have experimentally determined the anisotropic, linear viscoelastic behavior (for small oscillations) of the fiber-reinforced composite. Abarcar and Cunniff (1972) have formulated a discrete mathematical model to predict the natural frequencies and their corresponding mode shapes of fixed-free beams of general orthotropy. Huang and Teoh (1977) performed a theoretical analysis of the vibrations of fiber-reinforced composite beams using an energy approach. Hwang and

Gibson (1987) developed a micromechanical model to describe the damping in discontinuous fiber composites using strain energy approach. Teh and Huang (1979) presented finite element models for the prediction of natural frequencies of fixed-free beams of general orthotropy. Alberts and Xia (1995) developed a micromechanical model taking into account the effects of fiber segment lengths and relative motion between neighboring fibers. They showed that fiber-enhanced viscoelastic damping treatment provides significant damping to a treated cantilever beam.

Carbon nanotube (CNT) reinforced polymer composites are being widely investigated for damping purposes. Nikhil et al. (2003) studied the use of nanotube films in structures for vibration damping. He used nanotube films as inter-layers within composite piles. His experimental investigations revealed that by including nanotube films there is a 200% increase in damping levels. Zhou et al (2003) investigated the damping characteristics of polymeric composites distributed with single-walled carbon nanotubes**.** They demonstrated that single-walled carbon nanotube based composites achieve higher damping than composites with other types of fillers. Rios et. al. (2002) investigated the dynamical mechanical properties of single-walled nanotube reinforced polymer composites assuming a single linear solid model. Their work showed that there is a decrease in the loss factor with an increase in the percentage weight of carbon nanotubes. Further research has mainly focused on micromechanical modeling. Zhou et al (2004), described the load transfer between the CNTs and the resin using the concept of stick-slip motion. Thostenson and Chou (2003) used the micromechanical model used for modeling short fiber composites (Sun et al. 1985) to account for the structure of

nanotube reinforced composites. Liu and Chen (2003) demonstrated the boundary element method for modeling the micromechanical behaviour of CNT based composites.

Many modifications have been proposed to the topology of constrained layer structures in efforts to improve their damping performance. Multiple constrained layer treatments were suggested by Ungar and Ross (1959). Plunkett and Lee (1970) developed a method to compute the optimal section length of the constraining layer that provides maximum damping. Lin and Scott (1987) optimized the shape of a damping layer using a structural finite element model. Hajela and Lin (1991) used a global optimization strategy to maximize the system loss factor with respect to damping layer lengths for a constrained layer beam. The role of fibers in improving inherent damping in composite structures has been studied extensively by Gibson et al. (1982), Sun et al. (1985a) and Sun et al. (1985b). These studies involved analytical and experimental studies on aligned short fiber composites, aligned short fiber off-axis composites, and randomly oriented short fiber composites. Fiber aspect ratio, angle between applied tensile load and fiber direction, stiffness ratio between the fiber and matrix materials, and the damping ratio between fiber and matrix materials were optimized to improve damping in the structure. Alberts and Xia (1995) derived optimal relation between design parameters such as length, diameter, spacing and Young's modulus of fibers and shear modulus of viscoelastic matrix to achieve maximum damping performance.

Bendsøe and Kikuchi (1998) first introduced the homogenization method for finding the optimal topology for a structural problem. Topology optimization has been shown to be an efficient tool for structural problems with given boundary conditions. Vander Sluis, et al (1999) have performed topology optimization of heterogeneous

polymers using homogenization, but this study was purely static and did not examine damping properties. Yi, et al (2000) performed topology optimization using the homogenization method to maximize the damping characteristic of a viscoelastic material, but this was not in the context of constrained layer damping. Zeng et al (2003) performed layout optimization of passive constrained layer damping patches using a genetic algorithm based penalty function method. Three-phase composites have been studied in the context of optimizing thermal expansion for a composite (Sigmund and Torquato, 1997), but not in the context of constrained damping layer.

Lumsdaine (2002) successfully used topology optimization to find the optimal shape of a constrained viscoelastic damping layer with the objective of maximizing the system loss factor for the fundamental frequency of the base beam. A 325% improvement in the loss factor was achieved due to the material redistribution. Lumsdaine and Pai (2003) extended this work to perform base beam thickness and material fraction parameter studies. This involved performing optimization studies for different base beam thicknesses and material fractions. Significant improvements in the loss factor were obtained. The variations of the loss factor as the base beam thickness and material fraction were examined and the optimal base beam thickness and material fraction were determined. Pai et al, (2004) performed experimental validation of the results obtained from topology optimization studies. In this work, a configuration similar to the one used by Lumsdaine (2002) was used.

The optimization process requires calculation of gradients in every iteration. In all of the previous work (Lumsdaine 2002, Lumsdaine and Pai 2003 and Pai et al 2004), a finite difference based method was used which requires a finite element run for each

gradient calculation in an iteration. With a large number of design variables, this consumed a considerable amount of time (~30 hours) for the optimization. An aim of this study is to develop an analytical method for the gradient calculation in the optimization process. An analytical method would improve the efficiency of the optimization process as it would significantly reduce the number of finite element runs required per iteration. Additionally, NRP material is used in the core instead of purely viscoelastic material. Apart from the material fractions of NRP and elastic materials the volume fraction of nanotubes in the polymer is also allowed to vary in the optimization process.

1.2 Problem Statement

The objective of this work is to determine the best topology of a carbon nanotube reinforced polymer damping treatment so as to maximize the system loss factor for the fundamental frequency.

A constrained layer beam structure with a NRP (Nanotube Reinforced Polymer) core and an elastic constraining layer is used. The NRP core and the constraining layer constitute the design space in the optimization process. The beam is modeled using finite elements with two-dimensional second-order plane stress continuum elements. The material fractions of NRP and the elastic material in each of these finite elements and the volume fraction of carbon nanotubes in the polymer are the design variables. Analysis is done using the commercial finite element code ABAQUS. As the material fractions and volume fraction of CNTs change in the optimization process, the rule of mixtures is used to determine the material properties (stiffness and density) of the NRP core. A modified

modal strain energy method (Xu, et al, 2002) is used to compute the loss factor of the structure.

A gradient based optimization code (NLPQL) is used. Each time a new set of design variables are obtained, the objective (loss factor) and the gradients of the objective function with respect to the design variables are calculated analytically. A variation in the design variables affects the material properties (stiffness and density) of the corresponding elements. Hence, a finite element analysis is performed to obtain the new stiffness and mass matrices and the mode shape of the structure. These are then used to compute the elastic and viscoelastic strain energies of the structure. The newly computed stiffness and mass matrices, mode shape and strain energies are used to compute the loss factor and the gradients.

Parameters such as thickness of the base beam and the volume of the damping material and NRP material are varied and the effect of these parameters on the optimal shapes is examined. It is seen that there is a remarkable improvement in damping of about 1000% in the structure. This huge improvement in the damping levels is seen to be consistent for all the cases. This demonstrates the robustness of topology optimization. Moreover, in all the cases, the volume fraction of nanotubes increases to the maximum allowable value. As a result the NRP material becomes highly stiff. This high stiffness material no longer dissipates energy by shear and changes from being a constrained layer to being a free layer damping structure.

Chapter 2 gives an overview of the analytical and finite element modeling, the theory behind the problem and assumptions made, and also describes the implementation of the finite element model in the optimization algorithm. Chapter 3 explains the

analytical gradient calculation method. Chapter 4 shows the results –a comparison of the results obtained from analytical and numerical gradient calculation methods and the results of the parameter studies. The last chapter consists of the conclusions and a discussion of possible future work.

CHAPTER 2: MODELLING

This chapter gives an overview of the material modeling for the viscoelastic material and the NRP composite, the methods used to measure damping in the structure- the modal strain energy method and the half power bandwidth method, and the finite element modeling for the structure.

Carbon nanotube based polymer composites are being widely investigated for vibration damping purposes. Unlike purely elastic materials which have a lattice structure, a polymer material consists of long chain molecules. Due to the imperfect elasticity of these long chain polymers, the material gives much larger energy dissipation when deformed dynamically. Carbon nanotubes have stiffness of the order of 1 TPa. When a polymer matrix is reinforced with such high stiffness material, the resulting composite is assumed to exhibit greater stiffness due to the presence of nanotubes and greater energy dissipation due to the viscoelasticity of the polymer.

2.1 Material Modelling

2.1.1 Composite Properties

Many micromechanical models were used to describe the damping properties of nanotube reinforced polymer composites (see section 1.1). None of these material models are suitable to implement in a dynamic FE model as it requires both stiffness and damping properties of the composite which none of these models provide. Since a suitable model is not available in the literature a simplified model is adapted for this study. A better model will be implemented when one becomes available. It is assumed that the NRP composite behaves as a viscoelastic material with its material properties determined by the rule of mixtures (equations 2.1 and 2.2). Uniform distribution and

random orientation of nanotubes in the polymer matrix is assumed, i.e. the equivalent viscoelastic material is isotropic.

$$\rho = v_f \,.\, \rho_{NT} + \left(1 - v_f\right).\, \rho_v \tag{2.1}$$

$$E = v_f \,.E_{NT} + \left(1 - v_f\right).\, E_v \tag{2.2}$$

The material loss factor varies with the volume fraction of the nanotubes. Again, due to the unavailability of a model which sufficiently describes the effects of nanotube volume fraction on the loss factor, a constant material loss factor equal to the loss factor of the polymer matrix is assumed.

2.1.2 Viscoelasticity

Viscoelasticity may be defined as material response that exhibits characteristics of both a viscous fluid and an elastic solid. An elastic material returns to its original position instantaneously when stretched and released, whereas a viscous fluid such as putty retains its extended shape when pulled. A viscoelastic material combines these two properties, i.e., it returns to its original shape after being stressed and released, but does it slowly enough to oppose the next cycle of vibration. For elastic materials,

$$\sigma = E\varepsilon \tag{2.3}$$

And for viscoelastic materials under going harmonic excitation we have,

$$\sigma = E^* \varepsilon \tag{2.4}$$

where

$$E^* = \left(E' + iE''\right) \text{ or,} \tag{2.5}$$

$$E^* = E'\left(1 + i\eta_c\right) \tag{2.6}$$

where

E^* is the complex elastic modulus

E' is the elastic or storage modulus and

E'' is the loss modulus

$\eta_c = E''/E'$ is the material loss factor (2.7)

Unlike elastic materials where the stress and strain are in phase, in viscoelastic materials, the stress leads the strain by a phase angle depending on the loss factor η_c. A plot of stress versus strain for one cycle of oscillation is as shown in the figure 2.1. The area of this loop gives the amount of energy dissipated per cycle of oscillation. The loss factor is approximately twice the damping ratio of the system ($\eta_c \approx 2\xi$) for cases of light damping.

Apart from the elastic modulus, the shear modulus, bulk modulus and Poisson's ratio are also complex quantities for a viscoelastic material. They are given by equations,

$G^* = (G' + iG'')$ (2.8)

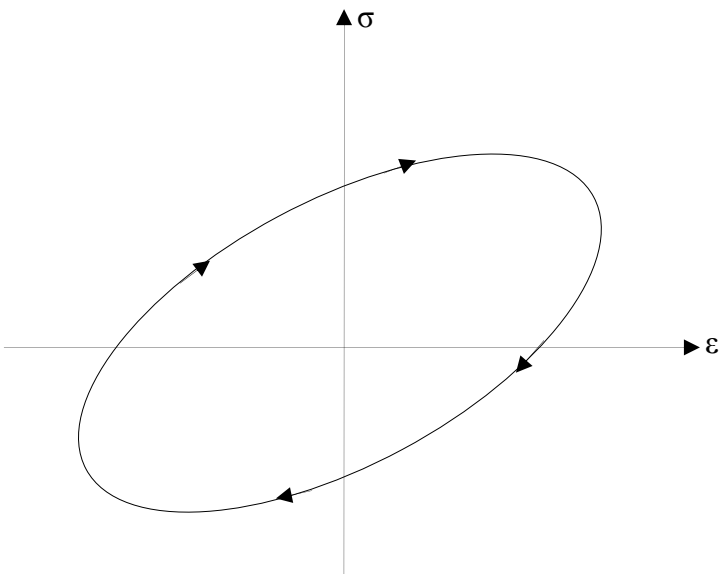

Figure 2.1 Elliptical hysteresis loop for linear viscoelastic materials

$$K^* = (K' + iK'') = \frac{E^*}{3(1-2\nu^*)} \tag{2.9}$$

$$G^* = \frac{E^*}{2(1+\nu^*)} \tag{2.10}$$

These viscoelastic properties are frequency dependent. Viscoelastic properties can be entered into ABAQUS (finite element code used in this work) in several ways. In the frequency domain, tabular values of G', G'', K', and K'', suitably normalized, can be entered as functions of frequency. Since the elastic modulus and Poisson's ratio may be related to the shear modulus and bulk modulus using equations (2.9) and (2.10) (even in a dynamic analysis), a varying Poisson's ratio can be taken into account when entering the shear and bulk moduli.

Very little Poisson's ratio data is available for viscoelastic materials in general. Often, viscoelastic materials are assumed to be incompressible (ν = 0.5) in regions of rubbery behavior and ν= 0.3 is assumed in regions of glassy behavior. The measurement of variation of the Poisson's ratio with frequency is very difficult to obtain experimentally and is not available for most damping materials. Hence, a constant Poisson's ratio of 0.4 is assumed in this work.

The material properties of viscoelastic materials are also dependent on the temperature. However these effects are not considered here.

2.2 System Loss Factor

2.2.1 Modal Strain Energy Method

Ungar and Kerwin (1962) defined the loss factor of a viscoelastic system in terms of strain energy quantities as,

$$\eta = \frac{U_u}{U} \tag{2.11}$$

where

η is the loss factor of a structure with layered viscoelastic damping.(system loss factor)

U_u is the portion of strain energy attributable to the viscoelastic core and

U is the strain energy of the system

The discretized equation of motion of a dynamic system is,

$$[\mathbf{M}]\{\ddot{x}\} + [\mathbf{C}]\{\dot{x}\} + [\mathbf{K}]\{x\} = \{\mathbf{F}\} \tag{2.12}$$

where

$[\mathbf{M}], [\mathbf{C}], [\mathbf{K}]$ are the mass, damping and stiffness matrices (all real and constant)

$\{x\}, \{\dot{x}\}, \{\ddot{x}\}$ are the vectors of nodal displacements, velocities and accelerations

$\{\mathbf{F}\}$ is the vector of applied loads

For a system with viscoelastic material, $[\mathbf{C}]$ can be neglected since the damping due to viscoelastic material is predominant and is accounted for by using $[\mathbf{K}] = [\mathbf{K1}]\{x\} + i[\mathbf{K2}]\{x\}$

Therefore the discretized equation of motion for a viscoelastic system is,

$$[\mathbf{M}]\{\ddot{x}\} + [\mathbf{K1}]\{x\} + i[\mathbf{K2}]\{x\} = \{\mathbf{F}\} \tag{2.13}$$

Solving this system gives complex eigenvalues and eigenvectors and is computationally expensive. Johnson and Kienholz (1981) developed the modal strain energy method which is an approximation to the complex eigenvalue method. The modal strain energy method assumes that the damped structure can be represented in terms of the real normal modes of the associated undamped system if appropriate damping terms (the material or

core loss factor) are inserted into the uncoupled modal equations of motion. Based on these assumptions the expression for loss factor was given as

$$\eta = \frac{U_u}{U} \approx \eta_c \frac{U_V}{U_V + U_E} = \eta_c \frac{\mathbf{\Phi}^T \left[\mathbf{K}^V\right] \mathbf{\Phi}}{\mathbf{\Phi}^T \left[\mathbf{K}^E + \mathbf{K}^V\right] \mathbf{\Phi}} \tag{2.14}$$

where

η_c is the loss factor of the viscoelastic core (material loss factor)

U_V is the strain energy of the viscoelastic elements obtained from purely elastic analysis

U_E is the strain energy of the elastic elements

$\mathbf{\Phi}$ is the eigen vector of the structure which is calculated from purely elastic analysis

$\mathbf{K}^E$ is the stiffness matrix of the elastic elements and

$\mathbf{K}^V$ is the stiffness matrix of the viscoelastic elements obtained from purely elastic analysis

Xu et al. (2002) revised the modal strain energy method to include the frequency dependence of the viscoelastic material. The loss factor as given by the revised modal strain energy method can be written as,

$$\eta = \eta_c \frac{\dfrac{U_V}{\sqrt{1 + \eta_c^2}}}{\dfrac{U_V}{\sqrt{1 + \eta_c^2}} + U_E}$$

Rearranging, we obtain

$$\eta = \frac{\eta_c \, U_V}{U_V + U_E \sqrt{1 + \eta_c^2}} \tag{2.15}$$

This expression for the loss factor of the structure is used in this study.

2.2.2 Half Power Bandwidth Method

The system loss factor may also be computed from the half-power bandwidth method as shown in figure 2.2, which requires obtaining the forced response over a wide frequency range (see Ewins, 2000):

$$\eta = \frac{\omega_2^2 - \omega_1^2}{2\omega_d^2} \tag{2.16}$$

where ω_1 and ω_2 are the frequencies at the half-power points. (i.e., at $A = A/\sqrt{2}$).

and ω_d is the damped natural frequency. In cases where the damping is light, the equation (2.11) reduces to,

$$\eta = \frac{\omega_2 - \omega_1}{\omega_d} \tag{2.17}$$

Unlike the modal strain energy (MSE) method which is an approximate method to compute the loss factor, the half power bandwidth method is an exact method. However, calculating loss factor by half power bandwidth (HPB) method requires calculating results at many points in a given frequency range, which in turn requires lengthy finite

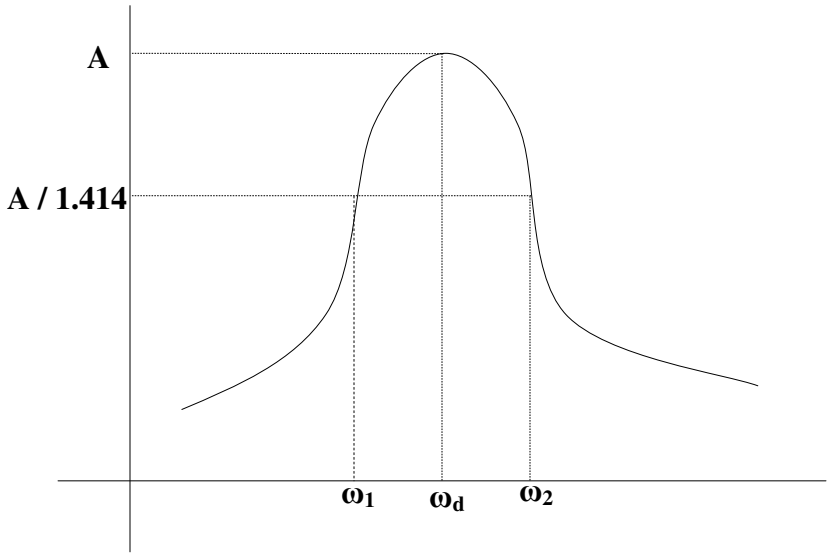

Figure 2.2 Half power bandwidth method

element calculations and makes the HPB much more computationally intensive to implement in an iterative process when compared to the MSE method. Moreover, viscoelasticity need not be included in the material modeling for the FE analysis while using the MSE method because MSE method uses the modes computed from an equivalent elastic model. However, loss factor of the structure at the start and at the end of the optimization is computed using the HPB method and compared with the loss factor calculations using MSE method.

The structure analyzed in this study is a cantilever beam modeled with two-dimensional plane stress continuum eight-noded quadratic elements. ABAQUS is used for the finite element analysis. Aluminum is used as the elastic material for the base layer and the constraining layer. The properties of the commercially available viscoelastic material (ISD 112 from 3M) are used for the polymer matrix material. Material properties used in this study are listed in table 2.1.

Table 2.1 Material properties

	Stiffness Modulus (GPa)	Density (kg/m^3)	Poisson's Ratio	Core loss factor
Elastic Material	68.9	2710	0.35	-
Viscoelastic Material	0.00281	1100	0.4	0.7
Carbon Nanotubes	1000	1400	0.4	-

CHAPTER 3: OPTIMIZATION

This chapter describes the optimization problem formulation, the flow chart for the optimization process and the analytical gradient formulation.

3.1 Problem Formulation

In this work, a simple material model is used, where the normalized density and modulus of the material for each element are allowed to vary together from 0% (in actuality, not zero but a very small value in order to prevent singularities in the stiffness matrix), which would be a "void," to 100%, which would represent 100% material. This is complicated by the fact that there are two material constituents – an elastic material and a NRP material. This is handled by placing two elements in the same location in the constraining layer design space – one that is NRP and one that is elastic. The density (and thus the modulus) of each element is allowed to vary from 0% to 100%, but the total density in each location (the density of the elastic element plus the density of the NRP element) is not allowed to be greater than 100%. Although this is artificial, in that it is unrealistic to consider manufacturing a structure with properties of two different materials (elastic and NRP), the results of this initial study lead to insight into the optimal constrained layer configuration, and could be used to develop a structure that is reasonable to manufacture.

The objective of this study is to maximize the system loss factor, measured using the modified modal strain energy method (equation 2.16). The design variables are the percentage of material in each element, where 0% represents a void, and 100% represents complete material (elastic or NRP, whichever the case may be). The result is validated by computing the loss factor using the half power bandwidth method. One constraint on the

objective is that the total fraction of each constituent in the constraining layer is fixed. (Technically, this is included as an inequality constraint rather than an equality constraint, but these constraints are virtually always active). For example, in one case, the NRP material is limited to be 20% of the total constraining layer design space, and the elastic material is limited to be another 20%. Furthermore, as mentioned above, the percentage of NRP material plus the percentage of elastic material must be less than or equal to 100% in each element location. To summarize, the optimization statement may be written as

Maximize η (system loss factor) such that

$$\frac{\sum_{i=1}^{n} x_i^v}{n} \leq f_v$$

$$\frac{\sum_{i=1}^{n} x_i^e}{n} \leq f_e$$

$$x_i^e + x_i^v \leq 1 \qquad i = 1,2,..n$$

$$1 \times 10^{-11} \leq x_i^e \leq 1 \qquad i = 1,2,..n$$

$$1 \times 10^{-7} \leq x_i^v \leq 1 \qquad i = 1,2,..n$$

$$1 \times 10^{-7} \leq v_f \leq 5 \times 10^{-2} \quad i = 1,2,..n$$

where

x_i^v is the fraction of NRP material of the element *"i"*

x_i^e is the fraction of elastic material of the element *"i"*

f_v is the total fraction of NRP material

f_e is the total fraction of elastic material

n is the number of NRP elements (which is equal to the number of elastic elements) and

v_f is the volume fraction of carbon nanotubes in the polymer material

Thus the material properties for a NRP/polymer material are (using equation 2.1 and equation 2.2)

$$\rho_i^v = x_i^v \left(v_f \times \rho_{NT} + \left(1 - v_f\right) \times \rho_v \right) \tag{2.19}$$

$$E_i^v = x_i^v \left(v_f \times E_{NT} + \left(1 - v_f\right) \times E_v \right) \tag{2.20}$$

The material properties for an elastic element are,

$$\rho_i^e = x_i^e \ \rho_e \tag{2.21}$$

$$E_i^e = x_i^e \ \mathrm{E}_e \tag{2.22}$$

The lower bounds on the material fractions of NRP elements are different from that for the elastic elements because the stiffness of the viscoelastic material varies by several orders of magnitude from that of aluminum. The volume fraction of nanotubes in the commercially available NRP is generally in the range of 0.1 to 5%. Hence in this study an upper limit of 5% is used for the volume fraction of nanotubes.

One difficulty in the optimization process is in finding the first bending mode. As the densities and the stiffnesses of the damping layer elements change, it is possible for new modes to appear locally. This happens when an elastic element is “floating in space”, (as shown in figure. 2.3) connected to the rest of the structure by elements that are at a very low stiffness. This results in a highly damped, low frequency mode that has no impact on

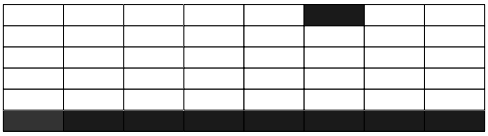

Figure 2.3 Finite element model producing local mode

the first mode of the base beam. Lumsdaine (2002) developed a heuristic in order to ensure that the mode whose loss factor is being optimized is truly the first mode of the beam, and not a local spurious mode. The first mode of the beam is one where the normalized displacement of the tip of the beam is large, while for the local spurious modes, displacements in the constraining layer are much larger than displacements at the tip of the beam. Additionally the first mode of the base beam generally does not change drastically between iterations, while the local spurious modes often have very low frequencies. These two quantities (normalized tip displacement and natural frequency) provide the most obvious clue as to which mode is the correct mode. Both need to be examined to identify the correct mode. If only the natural frequency is examined (as was done initially by Lumsdaine, 2000), then spurious modes develop at natural frequencies close to the frequency of the base beam. Thus, a criterion is developed that examines both the natural frequency and the normalized displacement. The inverse of the normalized tip displacement is added to the difference between the natural frequency of the mode in the current iteration and the natural frequency of the structure in the previous iteration of the optimization process. The first ten modes are examined, and the mode with the lowest value is chosen as the bending mode of the base beam. It should be noted that this quantity has no physical meaning. It has proven effective, however, in a variety of cases, to identify the proper mode of the beam.

The optimization flow chart is shown in figure 2.4. The initial values of the design

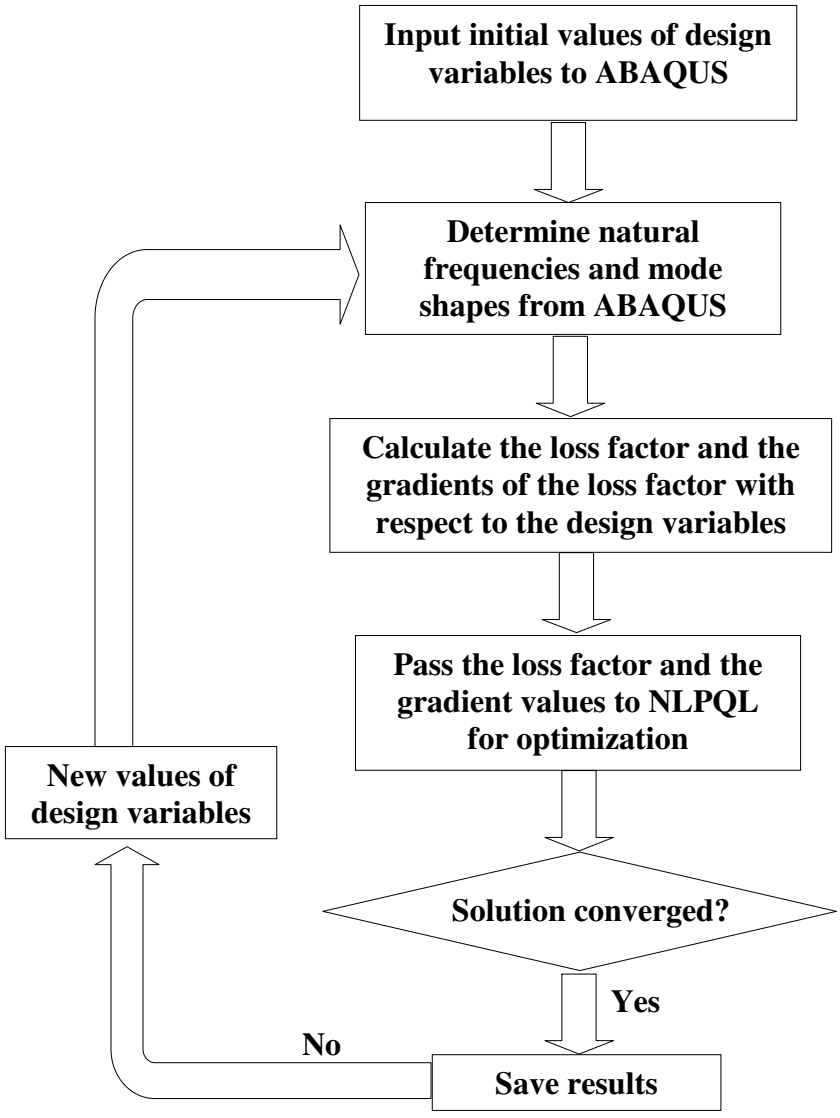

Figure 2.4 Optimization process flow chart

variables are used to compute the material properties of each of the finite elements. These material properties are then given to the finite element software (ABAQUS). The eigenvalue and eigenvector of the bending mode are obtained from the eigen analysis performed by ABAQUS. These values along with the stiffness and mass matrices are then used to compute the loss factor and the gradients of the loss factor with respect to each of the design variables. The values of the objective function (loss factor) along with the gradients are then input to NLPQL which is a gradient based optimization code. NLPQL then checks for convergence. If convergence is achieved, the process ends. If the convergence is not achieved, then it performs a line search to determine the next set of values for the design variables. These variables are then used to compute a new set of material properties to input to the finite element code.

3.2 Analytical Gradients Formulation

The most time consuming part of a gradient-based optimization process is the gradient calculations. With the increasing number of design variables, time taken for the gradient computation increases dramatically. In the previous studies (Lumsdaine, 2002 and Lumsdaine and Pai, 2003 Pai. et al., 2004) gradients were computed using the finite difference method.

$$\frac{\partial f}{\partial x_i} \cong \frac{f(\mathbf{x}+\Delta\mathbf{x}) - f(\mathbf{x})}{\Delta x_i}$$

where

Δx_i is the step size

$\frac{\partial f}{\partial x_i}$ is the gradient of the objective function with respect to the *i*th design variable

$f(\mathbf{x}+\Delta\mathbf{x})$ is the change in the objective function due to a small change in the *i*th variable

x is the vector [x_1 x_2 x_3 . . . x_n] ^{T} where x_i is the *i*th design variable

With "*n*" design variables, this involves "*n*" loss factor (objective) computations per iteration. Each loss factor computation requires a finite element run since the strain energies required to calculate the loss factor are obtained from the finite element analysis. Hence, each iteration in the optimization process requires as many finite element runs as the number of design variables. Moreover, a few more gradient calculations are required during the line search in the optimization process. With a large number of design variables, this consumes appreciable amount of CPU time. An alternative is to compute the gradients analytically so that only one finite element run is necessary per iteration (plus a few more runs for the line search).

The loss factor of a constrained layer damping structure using the modified modal strain energy method (Xu, et al, 2002) is given by equation 2.16

$$\eta = \frac{\eta_c \, U_V}{U_V \; + \; U_E \sqrt{1 \; + \; \eta_c^2}} \tag{3.1}$$

where

η_c is the core loss factor

U_V is the viscoelastic strain energy and

U_E is the elastic strain energy

The strain energies in terms of the elastic and viscoelastic stiffness matrices and the mode shape (Johnson and Kienholz, 1981) may be written as

$$U_V = \mathbf{\Phi}^T \mathbf{K}^V \mathbf{\Phi} \tag{3.2}$$

$$U_E = \mathbf{\Phi}^T \mathbf{K}^E \mathbf{\Phi} \tag{3.3}$$

where

$\mathbf{K}^V$ is the viscoelastic stiffness matrix of the structure

$\mathbf{K}^E$ is the elastic stiffness matrix of the structure and

$\mathbf{\Phi}$ is the eigenvector for the bending mode

The stiffness matrices and the mode shape can be obtained from the finite element analysis of the structure. And, since the core loss factor is assumed to be a constant value, the loss factor of the system can be computed. These stiffness matrices $\mathbf{K}^E$ and $\mathbf{K}^V$ are respectively the elastic and viscoelastic stiffness matrices for the structure.(The order of these matrices is equal to the number of degrees of freedom of the structure). Equations (3.2) and (3.3) can also be written as

$$U_V = \sum_{i=1}^{p} \mathbf{\Phi}_{iV}^T \mathbf{K}_i^V \mathbf{\Phi}_{iV} \tag{3.4}$$

$$U_E = \sum_{i=1}^{b} \mathbf{\Phi}_{iB}^T \mathbf{K}_i^B \mathbf{\Phi}_{iB} \quad + \quad \sum_{i=1}^{p} \mathbf{\Phi}_{iE}^T \mathbf{K}_i^E \mathbf{\Phi}_{iE} \tag{3.5}$$

where

$\mathbf{K}_i^V$, $\mathbf{K}_i^B$ and $\mathbf{K}_i^E$ are the elemental stiffness matrices of the *i*th viscoelastic element, *i*th elastic element in the base beam and *i*th elastic element in the design space, respectively

$\mathbf{\Phi}_{iV}$ is the part of the eigenvector for *i*th viscoelastic element

$\mathbf{\Phi}_{iB}$ is the part of the eigenvector for *i*th elastic element in the base beam element

$\mathbf{\Phi}_{iE}$ is the part of the eigenvector for *i*th elastic element in the design space

p is the number of viscoelastic elements = number of elastic elements in the design space

b is the number of elastic elements in the base beam

Note that, $\mathbf{K}_i^V$, $\mathbf{K}_i^B$ and $\mathbf{K}_i^E$ are 16x16 matrices (since the elements are eight noded elements with 2 degrees of freedom per node) and $\mathbf{\Phi}_{iV}$, $\mathbf{\Phi}_{iB}$ and $\mathbf{\Phi}_{iE}$ are vectors of length 16. Moreover, $\mathbf{\Phi}_{iV} = \mathbf{\Phi}_{iE}$ for i = 1..p, since the viscoelastic elements and the elastic elements in the design space are defined on the same nodes. Also, the base beam element stiffnesses are not affected by any of the design variables, since the base beam is not included in the design space. In other words, $\mathbf{K}_i^B$ for i = 1..b are all constant throughout the optimization. However, $\mathbf{\Phi}_{iB}$ changes as the mode shape of the structure changes.

The gradient of the loss factor can be computed by differentiating equation (3.1) with respect to the *i*th design variable,

$$\frac{\partial \eta}{\partial x_i} = \frac{\eta_c \sqrt{1 + \eta_c^2}\left\{ U_E \frac{\partial U_V}{\partial x_i} - U_V \frac{\partial U_E}{\partial x_i} \right\}}{\left[U_V + U_E \sqrt{1 + \eta_c^2} \right]^2} \tag{3.6}$$

Hence, to obtain the gradient of the loss factor with respect to the *i*th design variable, $\frac{\partial U_V}{\partial x_i}$ and $\frac{\partial U_E}{\partial x_i}$ need to be computed.

Differentiating the equations (3.2) and (3.3) with respect to design variable x_i yields

$$\frac{\partial U_V}{\partial x_i} = 2\left(\frac{\partial \mathbf{\Phi}}{\partial x_i}\right)^T \mathbf{K}^V \mathbf{\Phi} + \mathbf{\Phi}^T \frac{\partial \mathbf{K}^V}{\partial x_i} \mathbf{\Phi} \tag{3.7}$$

$$\frac{\partial U_E}{\partial x_i} = 2\left(\frac{\partial \mathbf{\Phi}}{\partial x_i}\right)^T \mathbf{K}^E \mathbf{\Phi} + \mathbf{\Phi}^T \frac{\partial \mathbf{K}^E}{\partial x_i} \mathbf{\Phi} \tag{3.8}$$

$\frac{\partial \mathbf{\Phi}}{\partial x_i}$, $\frac{\partial \mathbf{K}^E}{\partial x_i}$ and $\frac{\partial \mathbf{K}^V}{\partial x_i}$ still need to be determined to find the gradient of the loss factor. To find the derivative of the eigenvector of a matrix with respect to a design variable ($\frac{\partial \mathbf{\Phi}}{\partial x_i}$), a method proposed by Jung and Lee (1997) has been used and is described later in this chapter.

The terms $\mathbf{\Phi}^T \frac{\partial \mathbf{K}^V}{\partial x_i} \mathbf{\Phi}$ and $\mathbf{\Phi}^T \frac{\partial \mathbf{K}^E}{\partial x_i} \mathbf{\Phi}$ take different forms depending on whether the variable x_i is (a) material fraction of a viscoelastic element; (b) material fraction of elastic element; or (c) volume fraction of carbon nanotubes. Each of these possibilities is outlined below.

Case (a): $x_i = x_i^V$, material fraction of *i*th viscoelastic element.

In this case, $\mathbf{\Phi}^T \frac{\partial \mathbf{K}^E}{\partial x_i} \mathbf{\Phi} = 0$ since, a change in the material fraction of a viscoelastic element does not effect the elastic stiffness matrix and $\mathbf{\Phi}^T \frac{\partial \mathbf{K}^V}{\partial x_i} \mathbf{\Phi}$ can be expanded as,

$$\mathbf{\Phi}^T \frac{\partial \mathbf{K}^V}{\partial x_i} \mathbf{\Phi} = \mathbf{\Phi}_{1V}^T \frac{\partial \left(\mathbf{K}_1^V\right)}{\partial x_i^V} \mathbf{\Phi}_{1V} + .. + \mathbf{\Phi}_{iV}^T \frac{\partial \left(\mathbf{K}_i^V\right)}{\partial x_i^V} \mathbf{\Phi}_{iV} + .. + \mathbf{\Phi}_{pV}^T \frac{\partial \left(\mathbf{K}_p^V\right)}{\partial x_i^V} \mathbf{\Phi}_{pV} \tag{3.9}$$

Each of these elemental stiffness matrices ($\mathbf{K}_i^V$, i=1..p) varies linearly with the stiffness modulus of the corresponding element. The dimensions are constant throughout the optimization process but the stiffness modulus varies linearly as the material fraction as shown by equation (2.20)

$$E_i^V = x_i^V \left(v_f \times E_{NT} + \left(1 - v_f\right) \times E_v \right) \tag{3.10}$$

Therefore, the stiffness matrix of the *i*th element is directly proportional to the material fraction of that element and the matrix can be written as,

$$\mathbf{K}_i^V = x_i^V \mathbf{K}_{II} \tag{3.11}$$

where $\mathbf{K}_{II}$ is the stiffness matrix of a 100% viscoelastic element.

Using equation (3.11) in equation (3.9), we obtain

$$\mathbf{\Phi}^T \frac{\partial \mathbf{K}^V}{\partial x_i^V} \mathbf{\Phi} = \mathbf{\Phi}_{1V}^T \frac{\partial \left(x_1^V \mathbf{K}_{II} \right)}{\partial x_i^V} \mathbf{\Phi}_{1V} + .. + \mathbf{\Phi}_{iV}^T \frac{\partial \left(x_i^V \mathbf{K}_{II} \right)}{\partial x_i^V} \mathbf{\Phi}_{iV} + .. + \mathbf{\Phi}_{pV}^T \frac{\partial \left(x_p^V \mathbf{K}_{II} \right)}{\partial x_i^V} \mathbf{\Phi}_{pV}$$

All the terms in the above expansion goes to zero except $\mathbf{\Phi}_{iV}^T \frac{\partial \left(x_i^V \mathbf{K}_{II} \right)}{\partial x_i^V} \mathbf{\Phi}_{iV}$ .Therefore,

$$\mathbf{\Phi}^T \frac{\partial \mathbf{K}^V}{\partial x_i^V} \mathbf{\Phi} = \mathbf{\Phi}_{iV}^T \frac{\partial \left(x_i^V \mathbf{K}_{II} \right)}{\partial x_i^V} \mathbf{\Phi}_{iV} = \mathbf{\Phi}_{iV}^T \mathbf{K}_{II} \mathbf{\Phi}_{iV} \tag{3.12}$$

Using equation (3.12) in (3.7) yields

$$\frac{\partial \mathrm{U_V}}{\partial x_i^V} = 2 \left(\frac{\partial \mathbf{\Phi}}{\partial x_i^V} \right)^T \mathbf{K}^V \mathbf{\Phi} + \mathbf{\Phi}_{iV}^T \mathbf{K}_{II} \mathbf{\Phi}_{iV} \tag{3.15}$$

Case (b) :$x_i = x_i^E$, material fraction of *i*th elastic element.

In this case, $\mathbf{\Phi}^T \frac{\partial \mathbf{K}^V}{\partial x_i} \mathbf{\Phi} = 0$ and $\mathbf{\Phi}^T \frac{\partial \mathbf{K}^E}{\partial x_i^E} \mathbf{\Phi}$ can be expanded as

$$\mathbf{\Phi}^T \frac{\partial \mathbf{K}^E}{\partial x_i^E} \mathbf{\Phi} = \left(\sum_{i=1}^{b} \mathbf{\Phi}_{iB}^T \frac{\partial \mathbf{K}_i^B}{\partial x_i^E} \mathbf{\Phi}_{iB} \right) + \left(\mathbf{\Phi}_{1E}^T \frac{\partial \left(\mathbf{K}_1^E \right)}{\partial x_i^E} \mathbf{\Phi}_{1E} + .. + \mathbf{\Phi}_{iE}^T \frac{\partial \left(\mathbf{K}_p^E \right)}{\partial x_i^E} \mathbf{\Phi}_{iE} + .. + \mathbf{\Phi}_{pE}^T \frac{\partial \left(\mathbf{K}_p^E \right)}{\partial x_i^E} \mathbf{\Phi}_{pE} \right) \tag{3.16}$$

Here, $\left(\sum_{i=1}^{b} \boldsymbol{\Phi}_{iB}^{T} \frac{\partial \mathbf{K}_i^B}{\partial x_i^E} \boldsymbol{\Phi}_{iB} \right) = 0$ since the base beam elements are independent of the material fraction of the elements in the design space. Therefore,

$$\boldsymbol{\Phi}^T \frac{\partial \mathbf{K}^E}{\partial x_i^E} \boldsymbol{\Phi} = \boldsymbol{\Phi}_{1E}^T \frac{\partial \left(\mathbf{K}_1^E \right)}{\partial x_i^E} \boldsymbol{\Phi}_{1E} + .. + \boldsymbol{\Phi}_{iE}^T \frac{\partial \left(\mathbf{K}_i^E \right)}{\partial x_i^E} \boldsymbol{\Phi}_{iE} + .. + \boldsymbol{\Phi}_{pE}^T \frac{\partial \left(\mathbf{K}_p^E \right)}{\partial x_i^E} \boldsymbol{\Phi}_{pE} \tag{3.17}$$

Again, each of these elemental stiffness matrices ($\mathbf{K}_i^E$, i=1..p) vary linearly with the stiffness modulus of the corresponding element. The dimensions are constant throughout the optimization process but the stiffness modulus varies linearly as the material fraction as shown by equation (2.22)

$$E_i^E = x_i^E \,.\, E_e \tag{3.18}$$

Therefore, the stiffness matrix of the ith element is directly proportional to the material fraction of that element and the matrix can be written as

$$\mathbf{K}_i^E = x_i^E \mathbf{K}_{III} \qquad\qquad i = 1..p \tag{3.19}$$

where $\mathbf{K}_{III}$ is the stiffness matrix for a 100% elastic element in the design space.

Using equation (3.19) in equation (3.17) gives

$$\boldsymbol{\Phi}^T \frac{\partial \mathbf{K}^E}{\partial x_i^E} \boldsymbol{\Phi} = \boldsymbol{\Phi}_{1E}^T \frac{\partial \left(x_1^E \mathbf{K}_{III} \right)}{\partial x_i^E} \boldsymbol{\Phi}_{1E} + .. + \boldsymbol{\Phi}_{iE}^T \frac{\partial \left(x_i^E \mathbf{K}_{III} \right)}{\partial x_i^E} \boldsymbol{\Phi}_{iE} + .. + \boldsymbol{\Phi}_{pE}^T \frac{\partial \left(x_p^E \mathbf{K}_{III} \right)}{\partial x_i^E} \boldsymbol{\Phi}_{pE} \tag{3.20}$$

All the terms in the above expansion goes to zero except $\boldsymbol{\Phi}_{iE}^T \frac{\partial \left(x_i^E \mathbf{K}_{III} \right)}{\partial x_i^E} \boldsymbol{\Phi}_{iE}$. Therefore,

$$\boldsymbol{\Phi}^T \frac{\partial \mathbf{K}^E}{\partial x_i^E} \boldsymbol{\Phi} = \boldsymbol{\Phi}_{iE}^T \frac{\partial \left(x_i^E \mathbf{K}_{III} \right)}{\partial x_i^E} \boldsymbol{\Phi}_{iE} = \boldsymbol{\Phi}_{iE}^T \mathbf{K}_{III} \boldsymbol{\Phi}_{iE} \tag{3.21}$$

Using equation (3.21) in (3.8) yields

$$\frac{\partial \mathrm{U_E}}{\partial x_i^E} = 2\left(\frac{\partial \mathbf{\Phi}}{\partial x_i^E}\right)^T \mathbf{K}^E \mathbf{\Phi} + \mathbf{\Phi}_{iE}^T \mathbf{K}_{III} \mathbf{\Phi}_{iE} \tag{3.22}$$

Case (c): $x_i = v_f$, volume fraction of nanotubes in the viscoelastic material.

In this case, $\mathbf{\Phi}^T \frac{\partial \mathbf{K}^E}{\partial v_f} \mathbf{\Phi} = 0$ since volume fraction of nanotubes does not affect the elastic stiffness matrix and $\mathbf{\Phi}^T \frac{\partial \mathbf{K}^V}{\partial v_f} \mathbf{\Phi}$ can be expanded as

$$\mathbf{\Phi}^T \frac{\partial \mathbf{K}^V}{\partial v_f} \mathbf{\Phi} = \mathbf{\Phi}_{1V}^T \frac{\partial \left(\mathbf{K}_1^V\right)}{\partial v_f} \mathbf{\Phi}_{1V} + .. + \mathbf{\Phi}_{iV}^T \frac{\partial \left(\mathbf{K}_i^V\right)}{\partial v_f} \mathbf{\Phi}_{iV} + .. + \mathbf{\Phi}_{pV}^T \frac{\partial \left(\mathbf{K}_p^V\right)}{\partial v_f} \mathbf{\Phi}_{pV} \tag{3.23}$$

Differentiating $\mathbf{K}_i^V$ partially with respect to volume fraction of nanotubes gives

$$\frac{\partial \mathbf{K}_i^V}{\partial v_f} = \frac{\partial \mathrm{E}_i^V}{\partial v_f} \frac{\partial \mathbf{K}_i^V}{\partial \mathrm{E}_i^V}$$

E_i^V is given by, equation (2.0) as,

$$\mathrm{E}_i^V = x_i^V \left(v_f \times \mathrm{E}_{NT} + \left(1 - v_f\right) \times \mathrm{E}_V\right)$$

Therefore,

$$\frac{\partial \mathbf{K}_i^V}{\partial v_f} = x_i^V \left(\mathrm{E}_{NT} - \mathrm{E}_V\right) \cdot \frac{\mathbf{K}_i^V}{\mathrm{E}_i^V}$$

Equation (3.11) gives $\mathbf{K}_i^V = x_i^V \mathbf{K}_{II}$. Substituting this in the above equation and expanding E_i^V leads to

$$\frac{\partial \mathbf{K}_i^V}{\partial v_f} = x_i^V \left(\mathrm{E}_{NT} - \mathrm{E}_V\right) \cdot \frac{x_i^V \mathbf{K}_{II}}{x_i^V \left(v_f \times \mathrm{E}_{NT} + \left(1 - v_f\right) \times \mathrm{E}_V\right)}$$

Simplifying, we find

$$\frac{\partial \mathbf{K}_i^V}{\partial v_f} = x_i^V \frac{\left(\mathrm{E}_{NT} - \mathrm{E}_V\right)}{\left(v_f \times \mathrm{E}_{NT} + \left(1 - v_f\right) \times \mathrm{E}_V\right)} \cdot \mathbf{K}_{II} \tag{3.24}$$

Taking $C_K = \frac{\left(\mathrm{E}_{NT} - \mathrm{E}_V\right)}{\left(v_f \times \mathrm{E}_{NT} + \left(1 - v_f\right) \times \mathrm{E}_V\right)}$ gives

$$\frac{\partial \mathbf{K}_i^V}{\partial v_f} = x_i^V C_K \cdot \mathbf{K}_{II} \tag{3.25}$$

Using this in equation (3.23) yields

$$\mathbf{\Phi}^T \frac{\partial \mathbf{K}^V}{\partial v_f} \mathbf{\Phi} = C_K \sum_{i=1}^{p} x_i^V \mathbf{\Phi}_{iV}^T \mathbf{K}_{II} \mathbf{\Phi}_{iV}$$

Using this in equation (3.7) gives

$$\frac{\partial \mathrm{U_V}}{\partial v_f} = 2\left(\frac{\partial \mathbf{\Phi}}{\partial v_f}\right)^T \mathbf{K}^V \mathbf{\Phi} + C_K \sum_{i=1}^{p} x_i^V \mathbf{\Phi}_{iV}^T \mathbf{K}_{II} \mathbf{\Phi}_{iV}$$

Summarizing all the three cases, we have

$$\frac{\partial \eta}{\partial x_i} = \frac{\eta_c \sqrt{1 + \eta_c^2} \left\{ \mathrm{U_E} \frac{\partial \mathrm{U_V}}{\partial x_i} - \mathrm{U_V} \frac{\partial \mathrm{U_E}}{\partial x_i} \right\}}{\left[\mathrm{U_V} + \mathrm{U_E} \sqrt{1 + \eta_c^2} \right]^2} \tag{3.26}$$

$$\frac{\partial \mathrm{U_V}}{\partial x_i} = 2\left(\frac{\partial \mathbf{\Phi}}{\partial x_i}\right)^T \mathbf{K}^V \mathbf{\Phi} + \mathbf{\Phi}^T \frac{\partial \mathbf{K}^V}{\partial x_i} \mathbf{\Phi} \tag{3.27}$$

$$\frac{\partial \mathrm{U_E}}{\partial x_i} = 2\left(\frac{\partial \mathbf{\Phi}}{\partial x_i}\right)^T \mathbf{K}^E \mathbf{\Phi} + \mathbf{\Phi}^T \frac{\partial \mathbf{K}^E}{\partial x_i} \mathbf{\Phi} \tag{3.28}$$

For $x_i = x_i^V$ =material fraction of *i*th viscoelastic element.

$$\frac{\partial \mathrm{U_V}}{\partial x_i} = 2\left(\frac{\partial \mathbf{\Phi}}{\partial x_i}\right)^T \mathbf{K}^V \mathbf{\Phi} + \mathbf{\Phi}_{iV}^T \mathbf{K}_{II} \mathbf{\Phi}_{iV} \tag{3.29}$$

$$\frac{\partial U_E}{\partial x_i} = 2\left(\frac{\partial \mathbf{\Phi}}{\partial x_i}\right)^T \mathbf{K}^E \mathbf{\Phi} \tag{3.30}$$

For $x_i = x_i^E$, material fraction of ith elastic element.

$$\frac{\partial U_V}{\partial x_i} = 2\left(\frac{\partial \mathbf{\Phi}}{\partial x_i}\right)^T \mathbf{K}^V \mathbf{\Phi} \tag{3.31}$$

$$\frac{\partial U_E}{\partial x_i} = 2\left(\frac{\partial \mathbf{\Phi}}{\partial x_i}\right)^T \mathbf{K}^E \mathbf{\Phi} + \mathbf{\Phi}_{iE}^T \mathbf{K}_{III} \mathbf{\Phi}_{iE} \tag{3.32}$$

For, $x_i = v_f$, volume fraction of nanotubes in the viscoelastic material

$$\frac{\partial U_V}{\partial x_i} = 2\left(\frac{\partial \mathbf{\Phi}}{\partial x_i}\right)^T \mathbf{K}^V \mathbf{\Phi} + C_K \sum_{i=1}^{p} x_i^V \mathbf{\Phi}_{iV}^T \mathbf{K}_{II} \mathbf{\Phi}_{iV} \tag{3.33}$$

$$\frac{\partial U_E}{\partial x_i} = 2\left(\frac{\partial \mathbf{\Phi}}{\partial x_i}\right)^T \mathbf{K}^E \mathbf{\Phi} \tag{3.34}$$

To find the partial derivative of the eigenvector with respect to a design variable, $\frac{\partial \mathbf{\Phi}}{\partial x_i}$, a method proposed by Jung and Lee (1997) is used. This method is described below.

Step 1: Define $\mathbf{K}^* = \begin{bmatrix} \mathbf{K} - \lambda \mathbf{M} & -\mathbf{M}\mathbf{\Phi} \\ -\mathbf{\Phi}^T \mathbf{M} & 0 \end{bmatrix}$ (3.35)

where $\mathbf{K}$ is the global stiffness matrix, $\mathbf{M}$ is the global mass matrix and λ is the eigenvalue of the undamped system.

Here, $\mathbf{K} = \mathbf{K}^V + \mathbf{K}^E$ (3.36)

and $\mathbf{M} = \mathbf{M}^V + \mathbf{M}^E$ (3.37)

where $\mathbf{M}^{V}$ is the mass matrix of the viscoelastic elements and $\mathbf{M}^{E}$ is the mass matrix of the elastic elements. The elemental mass matrices $\mathbf{M}_i^V$ and $\mathbf{M}_i^E$ (16x16 matrices) for the viscoelastic and elastic elements, respectively, vary linearly as the density of the corresponding elements. The densities are linear functions of the material fraction and are given by equations (2.19) and (2.21) as

$$\rho_i^v = x_i^v \left(v_f \times \rho_{NT} + \left(1 - v_f\right) \times \rho_v \right)$$

$$\rho_i^e = x_i^e \ \rho_e$$

Therefore, as in the case of stiffness matrices, we define $\mathbf{M}_{II}$ as the mass matrix of a viscoelastic element with 100% material and $\mathbf{M}_{III}$ as the mass matrix of an elastic element in the design space with 100% material such that

$$\mathbf{M}_i^V = x_i^V \mathbf{M}_{II} \tag{3.38}$$

$$\mathbf{M}_i^E = x_i^E \mathbf{M}_{III} \tag{3.39}$$

and the partial derivative of a viscoelastic mass matrix of the *i*th element with respect to the volume fraction of nanotubes is,

$$\frac{\partial \mathbf{M}_i^V}{\partial v_f} = x_i^V C_M \ . \ \mathbf{M}_{II} \tag{3.40}$$

where $C_M = \dfrac{\left(\rho_{NT} - \rho_V\right)}{\left(v_f \times \rho_{NT} + \left(1 - v_f\right) \times \rho_V\right)}$

Step 2: Compute, $f_i = \left\{ \begin{array}{c} -\left(\dfrac{\partial \mathbf{K}}{\partial x_i} - \lambda \dfrac{\partial \mathbf{M}}{\partial x_i} \right) \mathbf{\Phi} \\ 0.5 \, \mathbf{\Phi}^T \dfrac{\partial \mathbf{M}}{\partial x_i} \, \mathbf{\Phi} \end{array} \right\}$ (3.41)

When the design variable is the material fraction of viscoelastic elements,

$$f_i = \begin{Bmatrix} -\left(\mathbf{K}_{II} - \lambda \mathbf{M}_{II}\right)\boldsymbol{\Phi}_{iV} \\ 0.5\, \boldsymbol{\Phi}_{iV}^T \mathbf{M}_{II}\ \boldsymbol{\Phi}_{iV} \end{Bmatrix} \tag{3.42}$$

When the design variable is the material fraction of elastic elements,

$$f_i = \begin{Bmatrix} -\left(\mathbf{K}_{III} - \lambda \mathbf{M}_{III}\right)\boldsymbol{\Phi}_{iE} \\ 0.5\, \boldsymbol{\Phi}_{iE}^T \mathbf{M}_{III}\ \boldsymbol{\Phi}_{iE} \end{Bmatrix} \tag{3.43}$$

When the design variable is the volume fraction of nanotubes,

$$f_i = \begin{Bmatrix} -\left(C_K \mathbf{K}^V - \lambda\, C_M \mathbf{M}^V\right)\boldsymbol{\Phi} \\ 0.5\, C_M \boldsymbol{\Phi}^T\, \mathbf{M}^V\ \boldsymbol{\Phi} \end{Bmatrix} \tag{3.44}$$

The first element of the vector f_i as given by equation (3.41) is a vector of length equal to the number of degrees of freedom (ndof) of the structure and the second element is a scalar. In the equations (3.42) and (3.43) the vectors $\left[-\left(\mathbf{K}_{II} - \lambda \mathbf{M}_{II}\right)\boldsymbol{\Phi}_{iV}\right]$ and $\left[-\left(\mathbf{K}_{III} - \lambda \mathbf{M}_{III}\right)\boldsymbol{\Phi}_{iE}\right]$ are vectors of length 16 and need to be expanded to the length of ndof. This is done differently for each element depending on the position of the element *i* in the structure.

Step 3: Compute $\begin{Bmatrix} \dfrac{\partial \boldsymbol{\Phi}}{\partial x_i} \\ \dfrac{\partial \lambda}{\partial x_i} \end{Bmatrix} = \mathbf{K}^{*\,-1} f_i$ (3.45)

Jung and Lee (1997) also proved the non-singularity of the matrix $\mathbf{K}^*$.

Substituting $\dfrac{\partial \boldsymbol{\Phi}}{\partial x_i}$ obtained from equation (3.45) in equations (3.29) through (3.34), we can obtain $\dfrac{\partial \mathrm{U_V}}{\partial x_i}$ and $\dfrac{\partial \mathrm{U_E}}{\partial x_i}$ for all the design variables. Using $\dfrac{\partial \mathrm{U_V}}{\partial x_i}$ and $\dfrac{\partial \mathrm{U_E}}{\partial x_i}$ in equation (3.6) gives all the gradients.

The analytical calculation of gradients has been coded in FORTRAN. Using the analytical gradients in the optimization process resulted in a much faster convergence An optimization process which took approximately 30 hours to converge when the gradients are calculated numerically, takes approximately 2 hours to converge when analytical gradients are used.

3.2.1 Validation

To validate the above procedure, optimizations were performed using both the numerical and analytical gradients on a configuration similar to one used in Pai et al., (2004) (shown in figure 3.1). This is a cantilever beam using viscoelastic material- ISD 112 from 3M (not an NRP) for the constrained layer and aluminum for the elastic constraining layer. The design space is discretized into 80 elements (5 rows of 16 elements each). An elastic and a viscoelastic element are defined in each of these 80 locations. The material fractions of each of these elements are the design variables. So, we have 160 design variables in the optimization process.

The initial configuration shown in figure 3.1 consists of 20% material fraction. This means that the total amount of viscoelastic material in the design space amounts to 20% of the total design space. Here, the first 16 elements (first layer) are 100% viscoelastic. This implies that in the optimization process, the material factions of the first 16 viscoelastic elements are one and the material fractions of the remaining (80-16) 64 viscoelastic elements are zero (In fact, a very small number, $1x10^{-7}$ is used to avoid singularities in the stiffness matrix). 20% material fraction also means that total amount of elastic material in the design space is 20%.

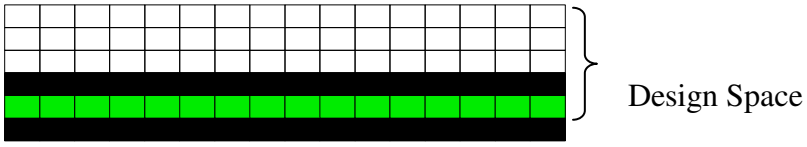

Figure 3.1 Initial configuration

Table 3.1 shows a comparison of the gradients calculated from numerical and analytical methods. Since we have 160 gradient calculations per iteration, only the first 25 gradients for the first iteration are shown. These are the gradients of the objective function with respect to first 25 viscoelastic elements.

It can be seen that the error for the first 16 values is less than 1%. From 17 to 25 (and further) the error is observed to be somewhat larger. This can be explained as follows. In the first iteration, the design variables 1 to 16 have a value 1 and the design variables 17 to 80 have a value $1x10^{-7}$. The step size in the numerical method is 0.005. Perturbing a design variable which has a value of 1 (design variables 1 till 16) by 0.005 gives an error close to zero, whereas perturbing a design variable which has a value close to zero ($1x10^{-7}$) by 0.005 make $(x+\Delta x) >> x$ and hence the error.

Using all x_i=0.2, an error close to zero for all the gradients has been observed. Gradients computed with all x_i=0.3, 0.5 0.7 have also been examined and the error was found to be close to zero for all the design variables.

Table 3.1 Comparison of gradients calculated from numerical and analytical methods

Design variable no.	Gradients using analytical method	Gradients using numerical method	Error
1	3.14E-05	3.16E-05	-0.57%
2	2.68E-04	2.68E-04	0.00%
3	6.23E-04	6.23E-04	0.01%
4	9.08E-04	9.08E-04	0.03%
5	1.07E-03	1.07E-03	0.10%
6	1.12E-03	1.12E-03	0.08%
7	1.10E-03	1.10E-03	0.10%
8	1.02E-03	1.02E-03	0.09%
9	8.99E-04	8.98E-04	0.07%
10	7.60E-04	7.59E-04	0.09%
11	6.13E-04	6.12E-04	0.04%
12	4.70E-04	4.69E-04	0.11%
13	3.45E-04	3.44E-04	0.03%
14	2.47E-04	2.46E-04	0.15%
15	1.83E-04	1.82E-04	0.22%
16	1.57E-04	1.56E-04	0.19%
17	-7.35E-06	-7.47E-06	-1.55%
18	-6.60E-06	-6.73E-06	-2.05%
19	-5.81E-06	-5.86E-06	-0.89%
20	-5.50E-06	-5.58E-06	-1.45%
21	-5.88E-06	-6.25E-06	-5.88%
22	-6.91E-06	-7.12E-06	-2.93%
23	-8.38E-06	-8.50E-06	-1.44%
24	-9.91E-06	-9.89E-06	0.25%
25	-1.11E-05	-1.17E-05	-5.02%

CHAPTER 4: RESULTS

This chapter contains a comparison of the results obtained from the optimization using analytical and numerical gradient calculation methods and the results for material fraction and base beam thickness parameter studies.

A comparison of the results from the topology optimization of the cantilever beam with the initial configuration shown in figure 3.1 using the analytical and numerical gradients methods in the optimization are as shown in the table 4.1. The viscoelastic and elastic material distribution at the end of the optimization are as shown in the figure 4.1. It can be seen that these are two different final shapes (although containing similar features). These could be two different local optima. Both the methods give approximately 1500% improvement in damping.

The optimization runs were performed on a Linux OS with Pentium dual core processor (3GHz) using ABAQUS6.5 for the finite element analysis. The optimization run using the numerical method completed in 31 hours 20 minutes and took 91 iterations, whereas the optimization run using the analytical method for gradient calculations completed in 2 hrs 30 minutes and took 581 iterations to converge.

Table 4.1 Comparison of results obtained from topology optimization using the analytical and numerical gradient calculation methods

	Analytical		Numerical	
	Initial	Final	Initial	Final
Natural frequency	42.64	0.0118	42.64	0.0118
Loss factor	46.49	0.1913	47.13	0.2102
% Imp.	1521.19		1681.36	
Time taken	2 hrs 30 min		31 hrs 20 min	
No. of iterations	581		91	

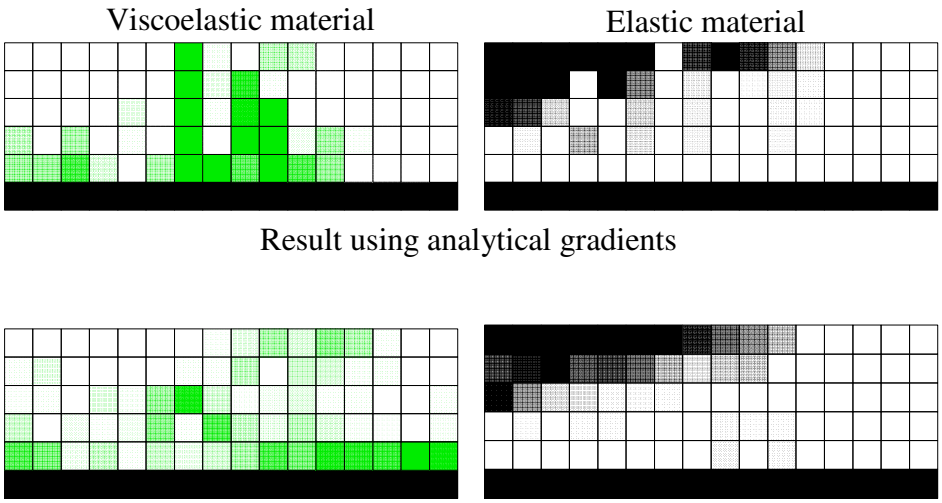

Figure 4.1 Final shapes

4.1 Parameter Studies

Parameter studies on a constrained layer beam using NRP material in the core are performed. The model used is a cantilever beam. The base beam is 75mm in length. The design space is 75mm x 0.5mm. The design space is divided into 5 layers of 8 elements each. Each element is 9.375 mm in length and 0.1 mm in height. The properties of the materials used in the optimization are listed in the table 4.2 (repeated from table 2.1). A constant core loss factor of 0.7 has been assumed for the NRP material.

The following parameter studies are performed:

1. Material fraction parameter study

2. Base beam thickness parameter study.

In these studies, the maximum amount of material in the design space and the thickness of the base beam are varied individually to determine the thickness and the amount of material that gives the best improvement in the loss factor and to show the robustness of the optimization process.

Table 4.2 Material properties (repeated from table 2.1)

	Stiffness modulus (GPa)	Density (kg/m^3)	Poisson's Ratio	Core loss factor
Elastic material	68.9	2710	0.35	-
Viscoelastic material	0.00281	1100	0.4	0.7
Carbon nanotubes	1000	1400	0.4	-

4.1.1 Material Fraction Parameter Study

In this study, the thickness of the base beam is held constant (0.5 mm) and the maximum amount of material allowed in the design space is varied from 10% to 50% of the design space. Topology optimization for each of these cases is performed.

At each of the 40 locations (5 rows x 8 elements) in the design space, there are two elements defined, elastic and NRP. This can be possible as long as the total material at each location does not go above 100%. A 20% material fraction would be equivalent to one full layer of NRP material and one full layer of elastic material. This is shown in figure.4.2. Similarly, for the 40% case we would have two layers filled with NRP material and 2 layers filled with elastic material. For the 10% case, we would have one layer of eight elements 50% NRP and 50% elastic material. Eight elements with 50% elastic material would be the same amount of material as four elements filled with 100% elastic material, which makes up 10% of the entire design space and the remaining 10% is the NRP material. The initial configurations for 10% and 20% case are shown in figure 4.2.

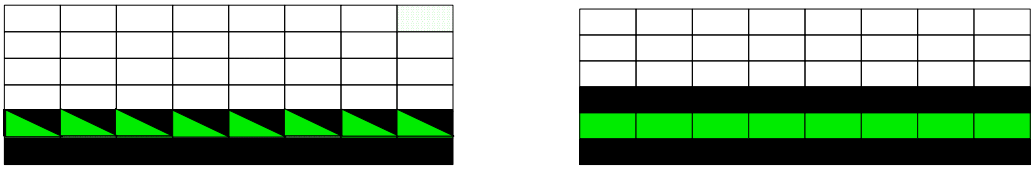

10% Material Fraction **20% Material Fraction**

Figure 4.2 Initial configurations

The results obtained from the topology optimization for all these cases are shown in table 4.3. The loss factor for the initial and final configurations is also computed using the Half power bandwidth method (HPB). These results are also shown for comparison. It can be seen that the percentage improvement in the damping loss factor is remarkably high at around 1000% for most cases.

Figure 4.3 shows the optimization results for the final densities for each case. The figure on the left shows the NRP composite material distribution in the design space for the optimal configuration and the figure on the right shows the elastic material distribution in the design space. The base beam is shown in black below the design space. The base beam has a thickness of 0.5 mm, which is the same as the design space thickness

but the heights of the design space elements are exaggerated for clarity. In some these figures the material seems to be floating in space. In actuality there is a very small amount of material (about 5%) between the material and the base beam –not large enough (to be significantly shown in the figures) but sufficient amount to keep the material connected to the base beam.

From the table 4.3 it can also be seen that a very significant improvement in the loss factor is achieved by topology optimization. However, this improvement is not uniform for 10% to 50% material fraction. From the final shapes in the figure 4.3 it can be seen

Table 4.3 Results obtained from modal strain energy method and half power bandwidth method for material fraction parameter study

Percentage of Material	Initial ω (Hz)	Initial η	Final ω(Hz.)	Final η	% Imp.
10% by MSE	158.86	0.0105	195.85	0.2359	2150%
10% by HPB	159.88	0.0125	223.09	0.1958	1463%
20% by MSE	167.72	0.0156	209.20	0.2912	1767%
20% by HPB	169.33	0.0185	243.94	0.2250	1116%
30% by MSE	181.57	0.0188	211.25	0.3046	1519%
30% by HPB	183.60	0.0222	248.33	0.2295	934%
40% by MSE	198.27	0.0182	194.34	0.3108	1611%
40% by HPB	200.50	0.0213	228.78	0.2333	995%
50% by MSE	214.77	0.0178	203.07	0.2946	1555%
50% by HPB	216.90	0.0208	238.46	0.2210	962%

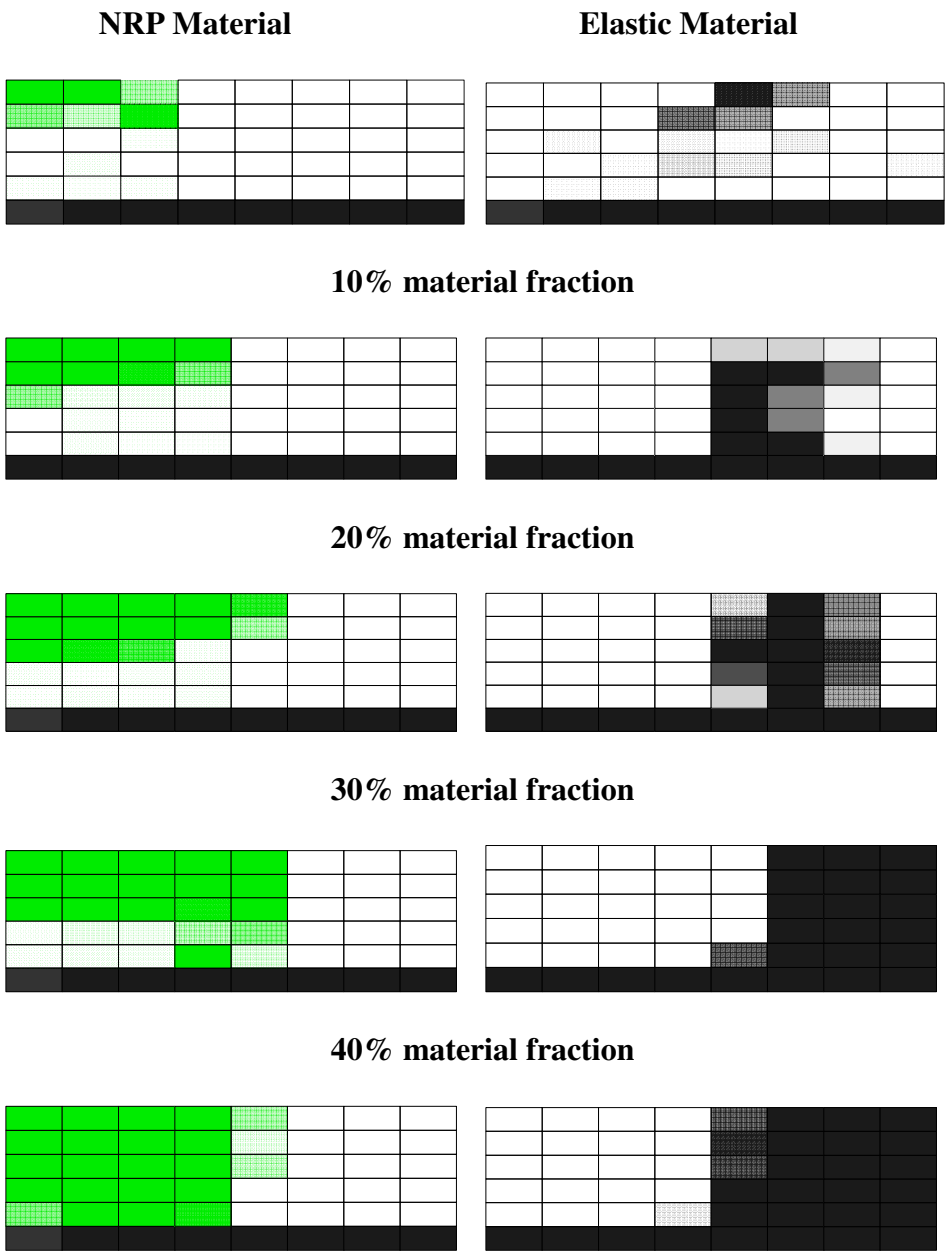

Figure 4.3 Material distribution in the optimized configuration for material fraction parameter study (heights of the damping layers are exaggerated)

that for 10% case all the NRP material accumulates at the root and top of the beam and a significant improvement in loss factor is observed. By the addition of more NRP material into the design space (20% till 50%) the NRP material accumulates around the same area, and the percentage improvement in loss factor decreases. This implies that the additional NRP material does not contribute much towards damping in the structure.

In all the cases, it has been observed that the volume fraction of the carbon nanotubes gradually moves towards the highest possible value. If the volume fraction were low, the NRP would be a low stiffness material and the dissipation of energy by shear could be more significant, but as the volume fraction of the carbon nanotubes increases, rendering very high stiffness to the material, the primary mechanism for the energy dissipation becomes extension rather than shear. It can be clearly seen that in all the above cases the NRP material, which now has stiffness almost the same as that of the elastic material, accumulates towards the root and the top of the cantilever beam. As the cantilever beam has the highest strain in this region, accumulation of the NRP material in this region indicates that the stiffness of the beam in this region is being increased.

Figure.4.4 and figure 4.5 shows the change in the loss factor in the initial and final configurations as the material fraction changes. It can be seen that the loss factors computed from the HPB and modal strain energy method (MSE) do not match but show the same trend. This difference can be attributed to the assumption in MSE method that the damped mode shape is identical to the undamped mode shape. Figure 4.6 shows the percentage increase in the loss factor from the initial to the final configurations.

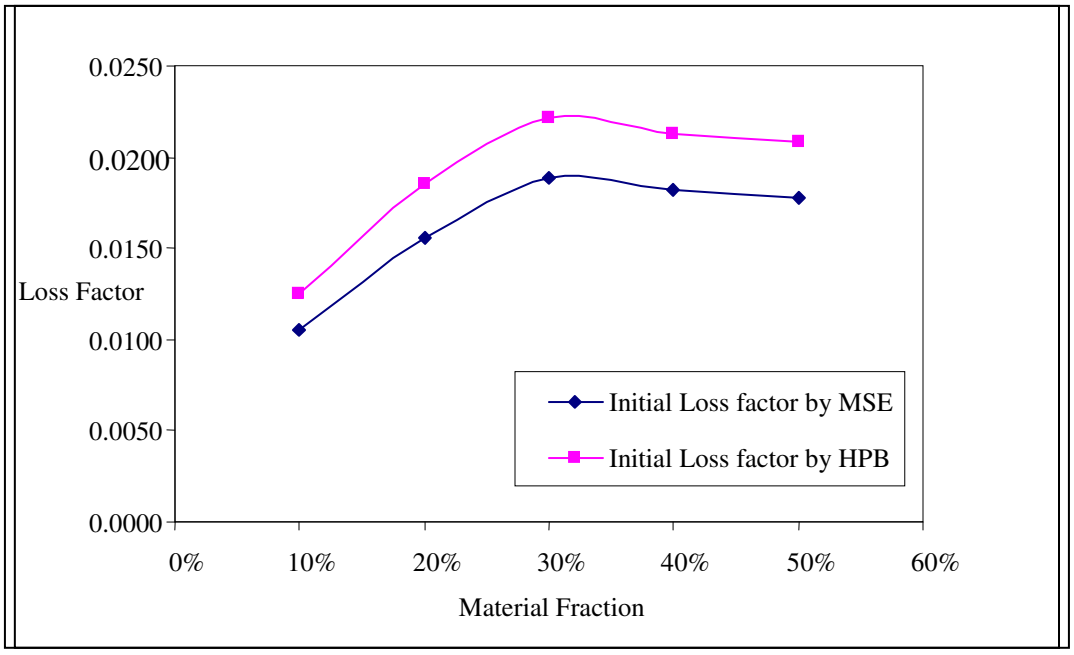

Figure 4.4 Initial loss factor vs. material fraction

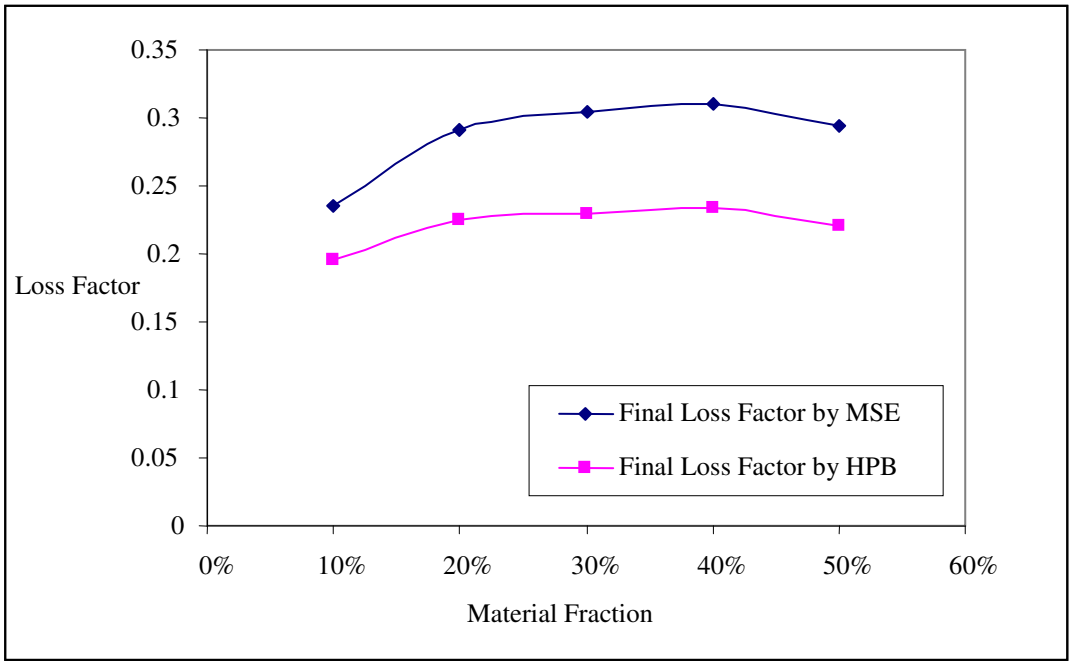

Figure 4.5 Final loss factor vs. material fraction

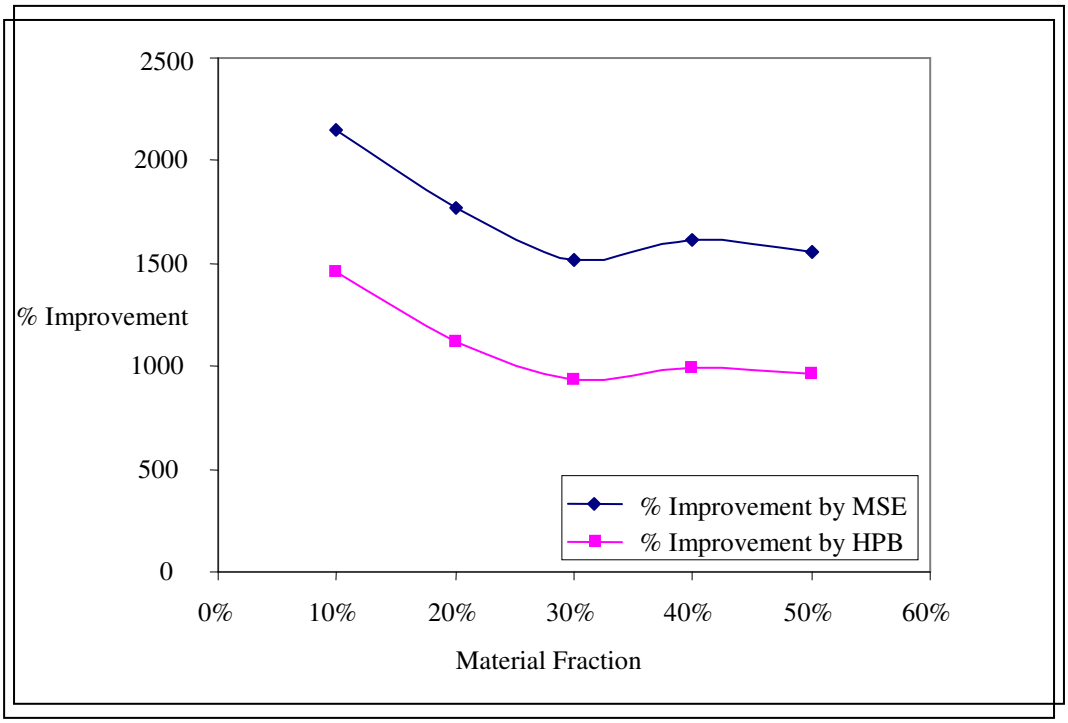

Figure 4.6 Percentage improvement in the loss factor vs. material fraction

4.1.2 Base Beam Thickness Parameter Study

In this study the maximum amount of material allowed in the design space is held constant (20% material fraction) and the base beam thickness is varied from 0.5 mm to 5mm. Optimization results for these cases are shown in table 4.4.

It can be observed from table 4.4 that a significant improvement in the loss factor can be obtained from the topology optimization of the structure and that the percentage improvement decreases as the thickness of the base beam increases. Figure 4.7 and figure 4.8 show the change in the loss factor in the initial and final configurations as the base beam thickness increases. It can be seen from these two plots that as the base beam thickness increases, the error in the loss factor calculated from the MSE method decreases, i.e., the loss factor from MSE and HPB methods come closer. This is intuitive

Table 4.4 Results obtained from modal strain energy method and half power bandwidth method for base beam thickness parameter study

Base beam Thickness	Initial ω(Hz)	Initial H	Final ω(Hz)	Final η	% Imp.
0.5mmbyMSE	99.2	0.0179	123.4	0.384	2047.49
0.5mmbyHPB	100.3	0.0211	148.9	0.266	1162.56
1mm by MSE	167.7	0.0156	203.4	0.276	1667.11
1mm by HPB	169.3	0.0185	235.7	0.216	1068.65
2mm by MSE	310.3	0.0100	343.5	0.159	1495.00
2mm by HPB	312.2	0.0119	376.7	0.148	1143.78
3mm by MSE	454.4	0.0072	490.3	0.110	1438.80
3mm by HPB	456.4	0.0087	523.3	0.110	1173.15
4mm by MSE	598.7	0.0057	623.3	0.086	1401.14
4mm by HPB	600.7	0.0067	654.9	0.086	1172.81
5mm by MSE	742.7	0.0045	773.2	0.062	1266.94
5mm by HPB	744.8	0.0055	801.1	0.065	1077.22

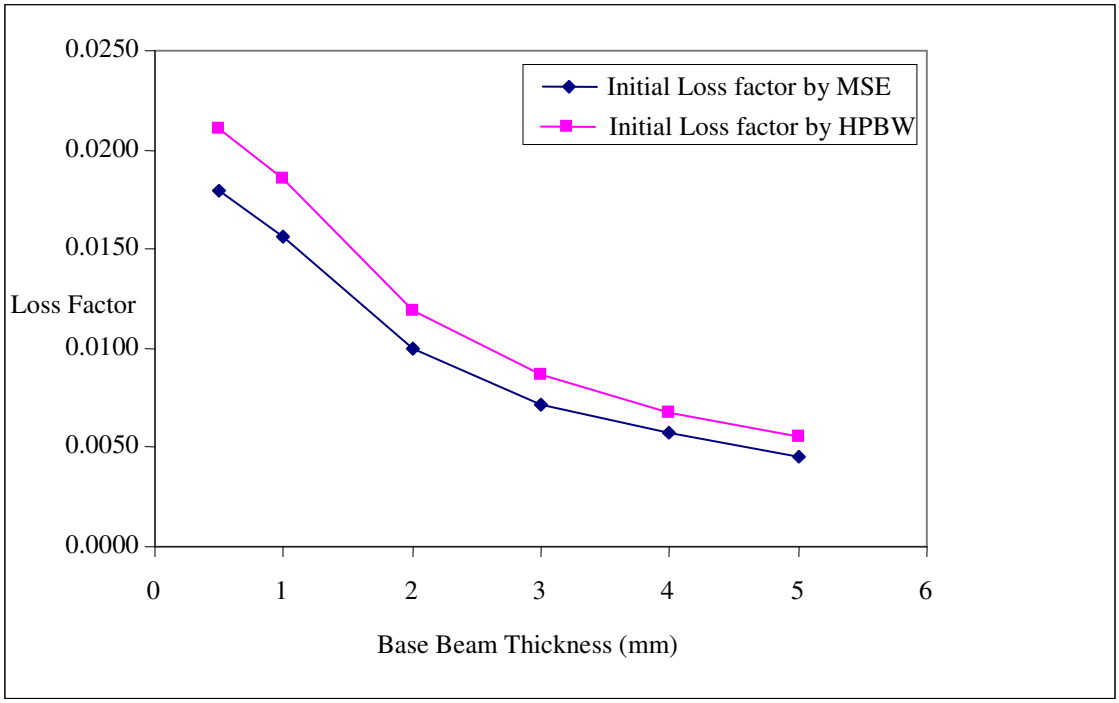

Figure 4.7 Initial loss factor vs. base beam thickness

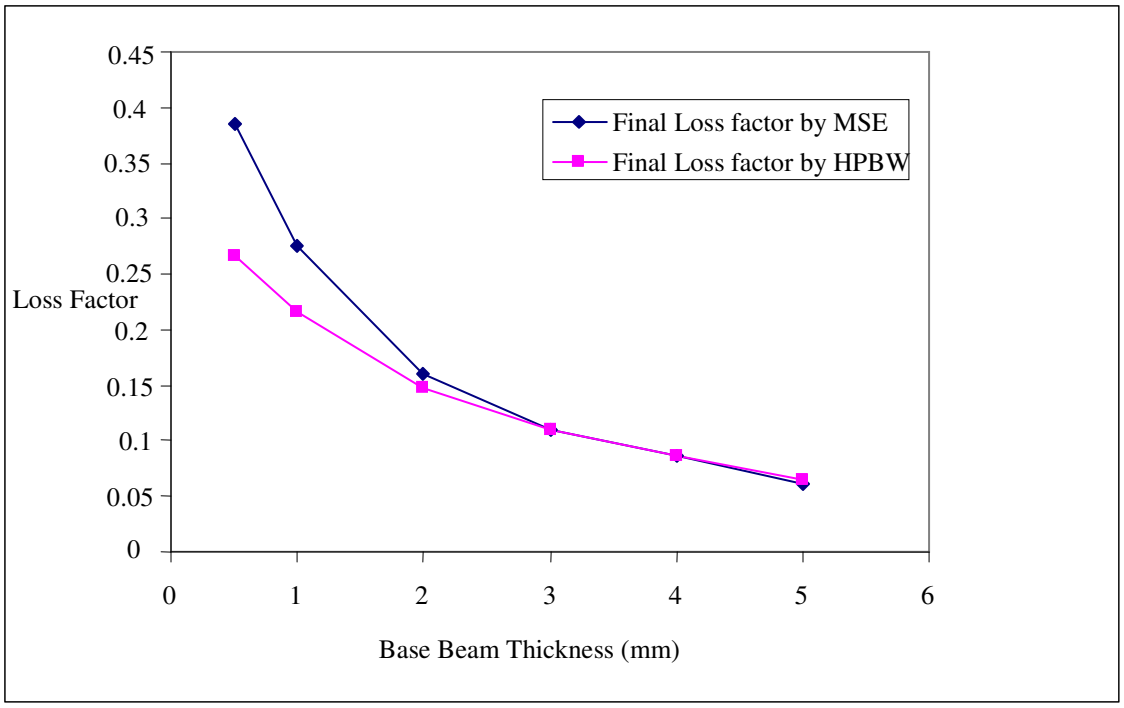

Figure 4.8 Final loss factor vs. base beam thickness

since, as the base beam thickness increases, the elastic part of the stiffness matrix dominates or the contribution of the imaginary part of the viscoelastic stiffness matrix to the loss factor decreases. Moreover, it is seen that the loss factor decreases as the base beam thickness increases. This is because there is less viscoelastic material than elastic material and therefore less damping in the structure. Figure 4.9 shows the percentage improvement in the loss factor as the base beam thickness increases. For the base beam thickness parameter study also, the composite material is seen to be moving toward the root of the cantilever beam (figure 4.10) thus stiffening the structure at the locations where there is higher strain due to extension.

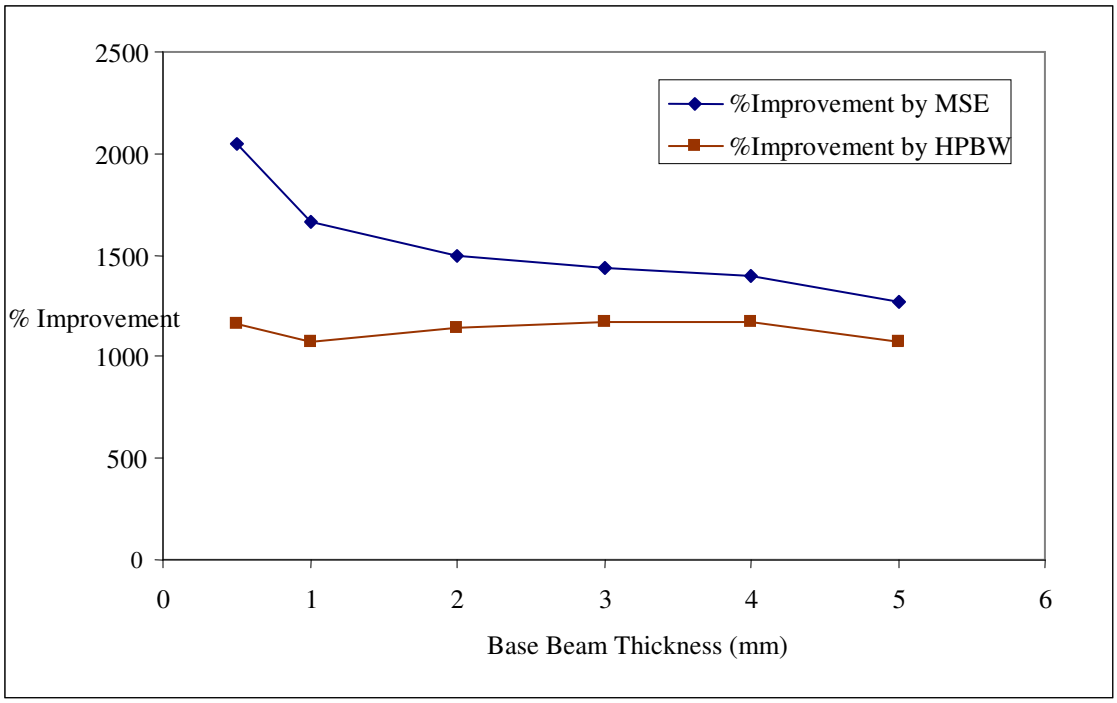

Figure 4.9 Percentage improvement in the loss factor vs. base beam thickness

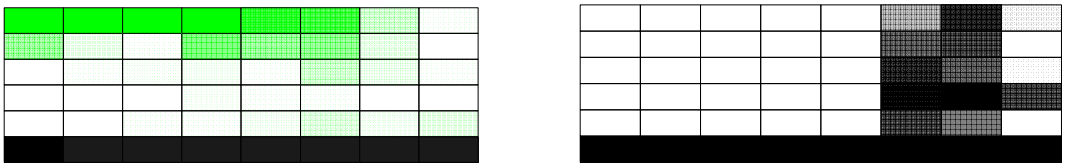

0.5 mm base beam thickness

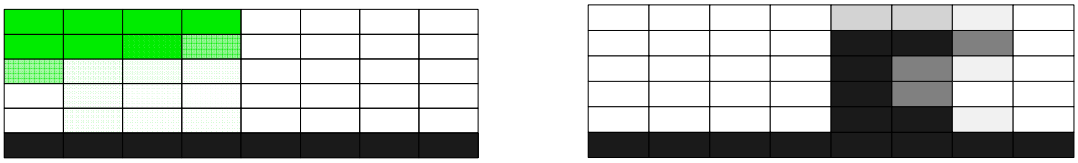

1 mm base beam thickness

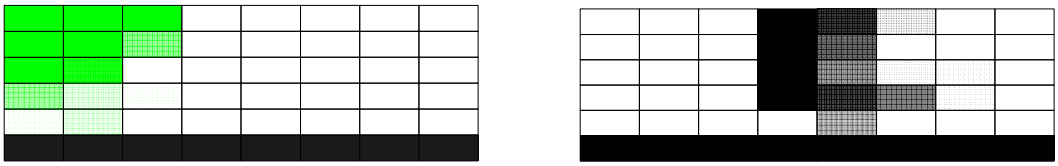

2 mm base beam thickness

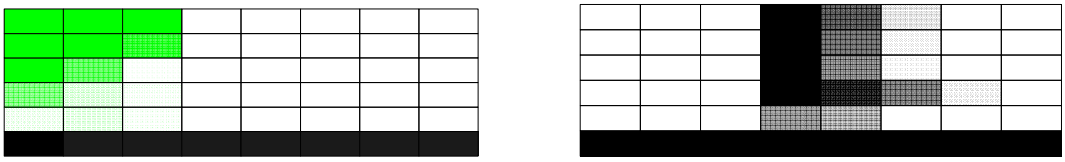

3 mm base beam thickness

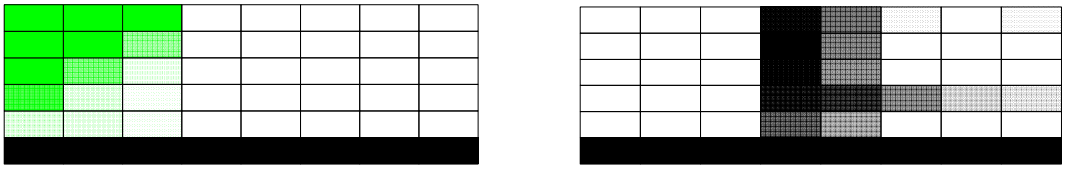

4 mm base beam thickness

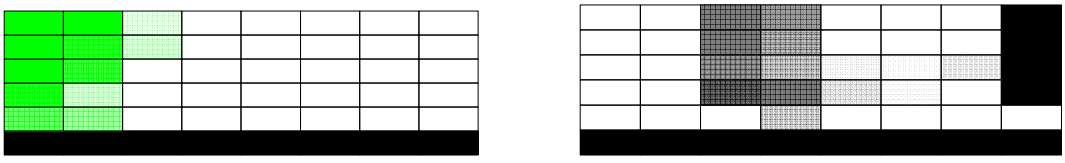

5 mm base beam thickness

Figure 4.10 Material distribution in the optimized configuration for base beam thickness parameter study (heights of the damping layers are exaggerated)

CHAPTER 5: CONCLUSIONS AND FUTURE WORK

The topology of a constrained damping treatment using NRP was optimized in order to maximize the loss factor of the structure. The optimized structures have shown a dramatic improvement of above 1000% in the loss factor in all the cases. It is seen that the NRP material moves toward the root and top of the cantilever beam and the volume fraction of the nanotubes reaches the highest possible value by the end of the optimization. Moreover the NRP material changes from being constrained layer to being a free layer. This implies that for the given materials, the energy dissipation is in the form of extension rather than shear. The increase in the volume fraction of nanotubes indicates that the material tends to stiffen itself. The normal stress is highest at the root of the cantilever beam and hence the high stiffness material moves towards the root of the beam.

Interpreting manufacturable shapes and testing them experimentally would validate the results obtained in this study. Moreover, a simplistic model (rule of mixtures) is used to model the composite material. In the absence of material models that take into account nano scale interactions of the polymer and nanotubes, using a micromechanical model could give reasonable results. Hwang and Gibson (1987) developed a micromechanical model to describe the damping in discontinuous fiber composites using a strain energy approach. Alberts and Xia (1995) investigated the properties of fiber enhanced viscoelastic polymer and derived an expression for the effective complex modulus of the new damping material using a micromechanical approach. Zhou et al. (2003) used stick-slip mechanism to characterize the energy dissipation and loss factor of a NRP material. A next step would be to examine/modify these models for applicability

in topology optimization. In this work a viscoelastic material is used for carbon nanotube reinforcement. In most of the studies, an epoxy was used. So using epoxy instead of a viscoelastic material is also a possible direction. Another option would be to examine ordinary fiber reinforced composites before using nano fiber reinforced composite materials.

Previously, the large amount of time consumed by the optimization process with the increase in the number of variables restricted the use of a large number of design variables. The development of the analytical gradient method improved the efficiency of the optimization process in that the time taken by the optimization process does not increase by a very large amount when the number of design variables is increased, as no additional finite element solutions are required, but only a gradient matrix calculation of a slightly larger order. Therefore, a finer meshing of the design space is possible. Inclusion of volume fraction and orientations of nanotubes in each of the element as design variables is also possible. A wider variety of materials can also be examined in less time.

Future studies can also include using the dimensions of the discretized elements as the design variables (shape optimization). For any given configuration, the solution found here might be a local optimum. Hence, using different optimization codes and algorithms such as VisualDoc, OptdesX, and MATLAB (optimization toolbox) might give better results and/or a better understanding of the problem.

Topology optimization that includes piezoelectric materials along with the NRP composites could be examined to obtain hybrid structures with much higher levels of damping.

BIBLIOGRAPHY

BIBLIOGRAPHY

Alberts T.E. and Xia H. 1995 "Design and Analysis of Fiber Enhanced Viscoelastic Damping Polymers", Journal of Vibration and Acoustics. Vol. 117, pp 398-404.

Abarcar R.B. and Cunniff P.F. 1972 "The Vibration of Cantilever Beams of Fiber Reinforced Material", Journal of Composite Materials. Vol. 6, pp 504 – 517.

Bendsoe M. P. 1995 Optimization of Structural Topology, Shape, and Material, pg. 10, Springer-Verlag.

DiTaranto R.A. 1965 "Theory of Vibratory Bending for Elastic and Viscoelastic Layered Finite-Length Beams", Journal of Applied Mechanics. pp 881-886.

Ewins, D. J. 2000 Modal Testing: Theory, Practice and Application, 2nd Edition, Research Studies Press, Ltd., Hertfordshire, England.

Gibson R.F., Chaturvedi S.K. and Sun.C.T.1982 "Complex Moduli of Aligned Discontinuous Fiber-Reinforced Polymer Composites", Journal of Material Science. Vol. 17 pp 3499-3509.

Huang C.C. and Teoh L.S. 1977 "The Vibration of Beams of Fiber Reinforced Material", Journal of Sound and Vibration Vol 51(4) pp 467-473.

Huang C.C. and Teh K.K 1979 "The Vibration of Generally Orthotropic Beams- A Finite Element Approach", Journal of Sound and Vibration Vol 62 (2) No.2 pp 195-206.

Hwang S. J. and Gibson R. F. 1987 "Micromechanical Modeling of Damping in Discontinuous Fiber Composites Using a Strain Energy /Finite Element Approach"., Journal of Engineering Materials and Technology. Vol 109 47-52.

Hwang S. J., Gibson R. F. and Singh J. 1992 “Decomposition of Coupling Effects on Damping of Laminated Composites Under Flexural Vibration”, Composites Science and Technology, Vol. 43, pp. 159-169.

Huang J. H. 2001 “Some Closed-Form Solutions for Effective Moduli of Composites Containing Randomly Oriented Short Fibers”, Materials Science and Engineering, A315, pp. 11-20.

Hajela P. and Lin C.Y. 1991 “Optimal Design of Viscoelastically Damped Beam Structures”, Applied Mechanics Review, 44 (11) - 2, pp. S96-S106.

Ioana C. F., Gary G. T. and Gibson R. F. 2003 “Modeling and characterization of damping in carbon nanofiber/polypropylene composites”, Composite Science and Technology., 63, pp 1629-1635.

Johnson C.D. and Kienholz D. A. 1981 “Finite Element Prediction of Damping in Structures with Constrained Viscoelastic Layers,” AIAA Journal, 20(9), pp. 1284 - 1290.

Kerwin E.M. Jr. 1959 “Ideal Spaced Damping Treatments for Flexural Waves”, Paper M10, Acoustical Society of America Spring Meeting,.

Liu Y.J. and Chen X.L. 2003 “Continuum Models of Carbon Nanotube-Based Composites Using the Boundary Element Method,” Electronic Journal of Boundary Elements, 1(2), pp.316-335.

Lekszycki T. and Olhoff N. 1981 “Optimal Design of Viscoelastic Structures Under Forced Steady-State Vibration,” The Journal of Structural Mechanics, 9. pp. 363-387.

Lall A.K., Nakra B.C. and Asnani N.T. 1983 “Optimum Design of Viscoelastically Damped Sandwich Panels”, Engineering Optimization, 6.pp. 197-205.

Lifshitz J.M. and Leibowitz M. 1987 “Optimal Samdwich Beam Design for Maximum Viscoelastic Damping”, International Journal of Solids and Structures, 23(7), pp. 1027 - 1034.

Lumsdaine A. and Scott R.A. 1998 “Shape Optimization of Unconstrained Viscoelastic Layers Using Continuum Finite Elements.” Journal of Sound and Vibration, 216(1), pp. 29-52.

Lumsdaine A. and Scott R.A. 1996, “Optimal Design of Constrained Plate Damping Layers Using Continuum Finite Elements”, Proceedings of the International Symposium on Advanced Materials for Vibro-Acoustic Application, 1996 American Society of Mechanical Engineers International Mechanical Engineering Congress and Exposition, Atlanta, GA, pp. 159-168.

Liu Q. and Chattopadhyay A. 2000 “Improved Helicopter Aeromechanical Stability Analysis Using Segmented Constrained Layer Damping and Hybrid Optimization,” Journal of Intelligent Material Systems and Structures, 11(6) pp.492-500.

Lumsdaine A. 2002 “Topology Optimization of Constrained Damping Layer Treatments”, ASME International Mechanical Engineering Congress & Exposition, New Orleans, Louisiana. IMECE2002-39021.

Lumsdaine A. and Pai R. 2003 “Design of Constrained Layer Damping Topologies,”Proceedings of the Adaptive Structures and Material Systems Symposium of the 2003 ASME International Mechanical Engineering Congress and Exposition, Washington, D.C.

Lundén R. 1979, “Optimum Distribution of Additive Damping of Vibrating Beams,” Journal of Sound and Vibration, Vol. 66, pp. 25-37.

Lundén R. 1980, “Optimum Distribution of Additive Damping of Vibrating Frames,” Journal of Sound and Vibration, Vol. 72, pp. 391-402.

Lee I. W. and Jung G.H. 1997 “An Efficient Algebraic Method for the Computation of Natural Frequency and Mode Shape Sensitivities – Part I. Distinct Natural Frequencies.” Computers & Structures, 62(3) , pp 429-435.

Mead D.J. and Markus S. 1969 “The Forced Vibrations of A Three-Layer, Damped Sandwich Beam with Arbitrary Boundary Conditions”, Journal of Sound and Vibration. Vol 10 pp 163-175.

Nakra B.C. 1976 “Vibration Control with Viscoelastic Materials.” Shock and Vibration Digest Vol 8, pp 3 -12

Nakra B.C. 1981 “Vibration Control with Viscoelastic Materials.” Shock and Vibration Digest Vol 13, pp 17 -20

Nakra B.C. 1984 “Vibration Control with Viscoelastic Materials.” Shock and Vibration Digest Vol 16, pp 17 -22

Nikhil A. K., Bingqing Wei and Pulickel M.A 2003 “Multifunctional Structural Reinforcement Featuring Carbon Nanotube Films”, Composite Science and Technology .63, pp.1525-1531.

Oberst H. and Frankenfeld K. 1952. “Uber die Damfug der Biegeshwingungen dunner Bleche dunch fest habtende Belage’s,” Acustica, Vol. 2, pp. 181-194.

Plunkett R. and Lee C. T. 1970 “Length Optimization for Constrained Viscoelastic Layer Damping”. The Journal of the Acoustical Society of America, 48(1), pp. 150-161.

Pai R., Lumsdaine A. and Parsons M. 2004 “Design and Fabrication of Optimal Constrained Layer Damping Topologies,” Proceedings of the SPIE 11th Annual Symposium on Smart Structures and Materials, San Diego, CA,

Ross D., Ungar E. Eric and Kerwin E.M. Jr. 1959 “Damping of Plate Flexural Vibrations by Means of Viscoelastic Laminae,” Structural Damping: Colloquium on Structural Damping, ASME Annual Meeting.

Rao D. K. 1978 “Frequency and Loss Factors of Sandwich Beams Under Various Boundary Conditions”, Journal of Mechanical Engineering Science, Vol. 20, No. 5, pp. 271-282.

Rios O., Fuentes A. A., Lozano K., Barrera E. V., and Brotzen F. R., 2002, "Dynamical Mechanical Study of Single Wall Nanotube Reinforced ABS Composites." Antec 2002, T 46: 3599-3603.

Rozvany G.I.N., Zhou M. and Birker T.1992 “Generalized Shape Optimization Without Homogenization,” Structural Optimization, 4 pp. 250-252.

Schultz. A. B. and Tsai. S. W. 1968 “Dynamic Moduli and Damping Ratios in Fiber-Reinforced Composites”, Journal of Composite Materials. Vol 2 No.3 pp368 – 379.

Soni M.L. and Bogner F.K.1981 “Finite Element Vibration Analysis of Damped Strucutres”, AIAA Journal Vol 20., N0.5 pp700-707.

Schittkowski K. 1986 “NLPQL: A FORTRAN Subroutine for Solving Constrained Non-linear Programming Problems,” Annals of Operations Research, 5, pp. 485 - 500.

Sun.C.T., Chaturvedi S.K. and Gibson R.F 1985 “Internal Damping of Short-Fiber Reinforced Polymer Matrix Composites”, Computers and Structures. Vol. 20 No 1-3 pp 391-400.

Sun.C.T., Chaturvedi S.K. and Gibson R.F 1985a "Internal Damping of Polymer Matrix Composites Under Off-Axis Loading", Journal of Material Science. Vol. 20 No 1-3 pp 391-400.

Sun.C.T., Wu, J.K. and Gibson R.F 1985b "Prediction of Material Damping in Randomly Oriented Short-Fiber Polymer Matrix Composites", Journal of Reinforced Plastics and Composites. Vol. 4 pp 262-272.

Thostenson E.T. and Chou T.W. 2003 "On The Elastic Properties of Carbon Nanotube-Based Composites: Modelling and Characterization", Journal of Physics D: Applied Physics. Vol 36 pp 573-582.

Ungar E.E. and Kerwin E.M. 1962 "Loss Factors of Viscoelastic Systems in Terms of Energy Concepts," Journal of the Acoustical Society of America, 34, pp. 954-957.

Ungar E.E and Ross. D. 1959 "Damping of Flexural Vibration by Alternate Viscoelastic and Elastic Layers," Proceedings of the Fourth Conference on Solid Mechanics, Unversity of Texas, Austin, Texas.

Vander Sluis O, Vosbeek P.H.J, Schreurs P.J.G, and Meijer H.E.H., 1999, "Homogenization of Heterogeneous Polymers," International Journal of Solids and Structures, 36, pp. 3193-3214.

Xu Y., Liu Y., and Wang B. 2002 "Revised Modal Strain Energy Method for Finite Element Analysis of Viscoelastic Damping Treated Structures," Proceedings of the SPIE 9th Annual Symposium on Smart Structures and Materials, 4697, pp. 35-42, San Diego, CA.

Yi, Y.-M., Park, S.-H. and Youn, S.-K. 2000 "Design of Microstructures of Viscoelastic Composites for Optimal Damping Characteristics," International Journal of Solids and Structures, Vol. 37, pp. 4791-4810.

Yang R. J. and Chuang C. H., 1994, "Optimal Topology Design Using Linear Programming," Computers and Structures, 52(2), pp. 265-275.

Zhou X., Shin E., Wang K. W. and Bakis C. 2003 "Damping Characteristics of Nanotube Based Composites," ASME 2003 Design Engineering Technical Conferences and Computers and Information in Engineering Conference. Chicago, IL.

Zhou X., Wang K. W. and Bakis C. 2004 "The Investigation of Carbon Nanotube Based Polymers for Improved Structural Damping," Proceedings of the SPIE 11th Annual Symposium on Smart Structures and Materials, San Diego, CA, 5386-18.

VITA

Seshadri Mohan Varma, Damu was born on 16th of July 1980 in a town called Narsapur, INDIA. He got his Bachelor of Engineering Degree from S.R.K.R. Engineering College, a college affiliated to Andhra University, INDIA. He obtained his Masters of Science Degree in Mechanical Engineering from the University of Tennessee in December 2005. He is currently working towards a PhD in Mechanical Engineering at the University of Tennessee, Knoxville.